Towards real-time imaging of single extracellular vesicle secretion by single cells

Ashlyn Leung

Department of Biomedical Engineering

McGill University, Montreal

March 2023

A thesis submitted to McGill University in partial fulfillment of the requirements of the degree of Master of Engineering

Table of Contents

Abstract

Extracellular vesicles (EVs) are membrane bound cell secretions that are said to play a key role in intercellular communication through the delivery of their cargo or detection of their surface markers. Although EVs are secreted by nearly all cell types, cancerous cells have been found to secrete many more EVs compared to heathy cells, as well as EVs of altered compositions. As such, the potential of EVs to be diagnostic biomarkers has been a growing field of research in recent years. Here, we describe two platforms designed for the isolation of single cells and direct imaging of their secreted EVs at a single particle level with the goal to associate EV secretion dynamics to cell physiology and pathology. The first platform is fabricated from a biocompatible hydrogel and consists of an array of microwells for isolation of single cells. In this set up, cells are attached to the ceiling of their microwells and secreted EVs bind to the surface below, all while being confined by the hydrogel so that EVs can be reassigned to their cell of origin. The second platform is a shallow flow cell fabricated from PDMS and dispenses with confining walls. Instead, the platform promotes spatial isolation of cells and relies on a narrow 25 μm gap between the capture substrate and secreting cells, allowing EVs to bind within a short radial distance of the secreting cell on the ceiling and be reassigned to their cell. Each platform's compatibility with extracellular matrix proteins to promote cell adhesion and ability to support long term culture of cells via media and nutrient exchange were characterized. EVs in the flow cell platform were captured by an antibody immobilized surface and imaged by confocal microscopy to achieve single EV resolution. To evaluate real-time imaging of single EVs, we incubated endogenously fluorescently labeled EVs at a concentration of 10^5 EVs/mL and tracked their binding to the capture surface over time. Finally, we demonstrate how EVs secreted directly from single cells can be detected in quasi real-time, limited by the diffusion lag and uncertainly within minutes. Our results indicate the potential of the monitoring platform to serve as a new tool for quantitative analysis of single cell EV secretion dynamics as a response to intracellular events.

Résumé

Les vésicules extracellulaires (VEs) sont des sécrétions cellulaires délimitées par une membrane qui jouent un rôle clé dans la communication intercellulaire par la livraison de leur contenu biomoléculaire ou la détection de leurs marqueurs de surface. Bien que les VEs soient sécrétées par presque tous les types de cellules, on a constaté que les cellules cancéreuses sécrètent beaucoup plus de VEs que les cellules saines, ainsi que des VEs de composition différente. Donc, le potentiel des VEs en tant que biomarqueurs diagnostiques a été un domaine de recherche croissant au cours des dernières années. Nous décrivons ici deux plateformes conçues pour l'isolement de cellules individuelles et l'imagerie directe de leurs VEs sécrétées au niveau de la particule unique, dans le but d'associer la dynamique de la sécrétion des VEs à la physiologie et à la pathologie des cellules. La première plateforme est composée d'un hydrogel biocompatible et comprend un réseau de micropuits pour l'isolement de cellules uniques. Dans cette configuration, les cellules sont fixées au plafond de leurs micropuits et les VEs sécrétés se lient à la surface en dessous, tout en étant confinés par l'hydrogel afin que les VEs puissent être réaffectés à leur cellule d'origine. La deuxième plate-forme est fabriquée à partir de PDMS et ne comporte pas de parois de confinement. Au lieu de cela, la plateforme favorise l'isolement spatial des cellules et s'appuie sur un espace étroit de 25 µm entre le substrat de capture et les cellules sécrétrices, ce qui permet aux VEs de se fixer à une courte distance radiale de la cellule sécrétrice sur le plafond et d'être réaffectés à leur cellule. La compatibilité de chaque plateforme avec les protéines de la matrice extracellulaire pour favoriser l'adhésion cellulaire et la capacité à supporter la culture à long terme de cellules par l'échange de milieux et de nutriments ont été caractérisées. Les VEs dans la plateforme de chambre PDMS ont été capturés par une surface couverte d’anticorps immobilisée et imagées par microscopie confocale pour résoudre les VEs individuelles. Enfin, pour évaluer l'imagerie en temps réel des VEs uniques, nous avons incubé des VEs marqués par fluorescence de façon endogène à une concentration de 10^5 VEs/mL et suivi leur liaison à la surface de capture au fil du temps. Enfin, nous démontrons comment les VEs sécrétées directement par des cellules uniques peuvent être détectées en quasi-temps réel, limitées par le délai de diffusion et l'incertitude en quelques minutes. Nos résultats indiquent le potentiel de la plateforme de suivi à titre de nouvel outil pour l'analyse quantitative de la dynamique de la sécrétion des VEs provenant de cellules individuelles en réponse à des événements intracellulaires.

Acknowledgements

First and foremost, I would like to thank my supervisor, Prof. David Juncker, for the invaluable guidance, feedback, and mentorship he's provided throughout the course of my project. Without his support, this work would not have been possible.

Many thanks to Dr. Andy Ng for his continued input on my project and insightful suggestions, Dr. Andreas Wallucks for his assistance in experimental planning and data analysis, and Dr. Félix Lussier for his mentorship, extensive knowledge, and discussions that never lacked in fun. I am also grateful to all the Juncker Lab members, in particular Geunyong Kim, Alan Huang, Molly Shen, Zijie Jin, Bisan Samara, and Vahid Karamzadeh, for always offering their help and feedback, and for their friendship which made this journey more rewarding.

Lastly, I would like to express my appreciation to my friends and family. Lynda Au and Gabriella Kong, thank you for welcoming me to Montreal, for your ongoing support, and for celebrating my little wins along the way. And thank you to my parents, and my brother, Curtis, for their constant encouragement and for always believing in my success.

I also wish to acknowledge the financial support from the Biomedical Engineering Department at McGill University through the Recruitment Award, and from NSERC through the CGS-M Award.

List of figures

List of abbreviations

AB	Apoptotic body
AHA	L-azidohomoalanine
APD	Avalanch photodiodes
BSA	Bovine serum albumin
CD*x*	Cluster of differentiation *x*
CFSE	Carboxyfluorescein diacetate succinimidyl ester
CTC	Circulating tumor cell
CTDR	CellTracker deep red
CuAAC	Copper catalyzed azide-alkyne cycloaddition
Del-1	Developmental endothelial locus-1
DIC	Differential interference contrast
DMEM	Dulbecco's Modified Eagle Medium
DNA	Deoxyribonucleic acid
ECM	Extracellular matrix
ED	Extracellular domain
ELISA	Enzyme linked immunosorbent assay
EpCAM	Epithelial cell adhesion molecule
ESCRT	Endosomal sorting complex required for transport
EV	Extracellular vesicle
FBS	Fetal bovine serum
FITC	Fluorescein isothiocyanate
FOV	Field of view
GFP	Green fluorescent protein
GLUT1	Glucose transporter 1
GRP78	78 kDa Glucose-regulated protein
HER2	Receptor tyrosine-protein kinase erbB-2
HMA	Hydrogel microwell array
HMW	High molecular weight
HPA	Hydroxypropyl acrylate
HSC70	70 kDa Heat shock conjugate
HSP*x*	*x* kDa Heat shock protein
ID	Inner diameter
ILV	Intraluminal vesicle
IPA	Isopropanol
iSCAT	Interferometric scattering
ISEV	International Society for Extracellular Vesicles
LAP	Lithium phenyl-2,4,6-trimethylbenzoylphosphinate
LDH-C4	Lactate Dehydrogenase-C4

LMW	Low molecular weight
LO	Large oncosomes
LOD	Limit of detection
MCF	Michigan Cancer Foundation
MS	Mass spectrometry
MV	Microvesicle
MVB	Multivesicular body
NTA	Nanoparticle tracking analysis
OSCC	Oral squamous cell carcinoma
PBS	Phosphate buffered saline
PCR	Polymerase chain reaction
PDMS	Polydimethylsiloxane
PEG	Poly(ethylene glycol)
PEGDA	Poly(ethylene glycol) diacrylate
PlGF	Placental growth factor
PM	Plasma membrane
PME	Premetasatic niche
POC	Point of care
PS	Penicillin-streptomycin
PTFE	Polytetrafluoroethylene
RNA	Ribonucleic acid
ROI	Region of interest
SFC	Shallow flow cell
SEM	Standard error of means
SP-IRIS	Single Particle Interferometric Reflectance Imaging Sensor
STORM	Stochastic Optical Reconstruction Microscopy
TIRFM	Total Internal Reflection Fluorescence
TME	Tumor microenvrionment
TSG101	Tumor susceptibility gene 101
TYRP-2	Tyrosinase-related protein-2
UV	Ultraviolet
VAUM	Vacuum assisted UV micromolding
VEGF	Vascular endothelial growth factor
VLA-4	Very late antigen 4
WDM	Wavelength division multiplexing

1. Introduction

1.1. Motivation

Extracellular vesicles (EV) are increasingly studied for their role in intercellular communication and value in clinical diagnostics[1]. EVs carrying numerous molecular information, such as proteins and nucleic acids, circulate in body fluids and are said to represent a fingerprint of their parent cell[2]. When the parent cell is cancerous, proteins on secreted EVs have been identified to be differentially expressed and different in abundance compared to healthy cells [1,3–5]. Therefore, EVs have emerged as a promising prospect for cancer diagnostics. Beyond the heterogeneity between healthy and diseased cells, as revealed by single cell sequencing and proteomics, heterogeneity of individual EVs has also been found to be unexpectedly high[6–8]. Technical limitations of most existing approaches do not allow the direct detection of single EVs from single cells to uncover said heterogeneity and lack temporal resolution to capture short-term responses of cells to drugs and environmental changes. As a result, there is limited understanding how both individual EV proteomics and EV secretion rate can reflect a cell's pathological state. EV heterogeneity could confound analysis and biomarker discovery; thus, it is important to map the heterogeneity of individual EVs from single cells with high temporal resolution to derive tumor cell heterogeneity.

1.2. Project goals

The overall goal of this project is to develop a platform to track and count the single EVs secreted by single cells. The resulting platform will enable the study of EV heterogeneity and secretion dynamics by conducting time-lapse studies on single cells. The first challenge is to isolate single cells and their secreted EVs while still enabling media exchange to the cells and the second challenge is to capture time course images of EV secretions at the single particle level. This project

will describe the design, fabrication, and characterization of two platforms suitable for the real-time analysis of single EVs secreted by single cells.

1.3. Contribution of Authors

For the present thesis, Ashlyn Leung designed and performed all experiments and the majority of the data analysis. Programming for data analysis was done with the help of Drs. Andreas Wallucks and Félix Lussier. 293T-GFP cells used in the reported experiments were provided by Molly Shen. The particle tracing simulations were performed in collaboration with Geunyong Kim. Prof. David Juncker supervised this project and provided guidance throughout its development. The thesis and accompanying figures were prepared by Ashlyn Leung and edited with the help of Prof. David Juncker and Dr. Andy Ng.

2. Comprehensive review of the relevant literature

2.1. Extracellular vesicles

Extracellular vesicles (EVs) are lipid bilayer membrane bound particles of various sizes, secreted by nearly all cell types into the extracellular space[8]. They carry various biological cargo such as lipids, nucleic acids, and proteins, and through the transfer of their cargo to recipient cells or detection of their specific surface markers, EVs play an important role in dictating intercellular communication and the regulation of physiological processes[9]. Depending on the physiological and pathological state of the cell, the EVs they secrete, and their associated cargo, can be altered[10,11]. As a result, there has been growing interest in the analysis of EVs for early disease detection and more recently, as universal biomarkers for cancer diagnostics and monitoring7

2.1.1. EV subtypes

As EV research has grown exponentially in the last several decades, the International Society for Extracellular Vesicles (ISEV) established minimum requirements for the definition of extracellular vesicles and their functions to improve the reliability and reproducibility of EV results among the scientific community[12]. “Extracellular vesicle” is the generic term used to describe particles that are naturally released from a cell that cannot replicate and are enclosed in a lipid bilayer. EVs can further be classified into the subtypes typically based on their size and biogenesis pathway (Figure 1). However, due to the difficulty in tracing EV biogenesis pathways, the use of operational terms for EV subtypes that refer to physical size, such as “small EVs” and “medium or large EVs”, have become more common. Although the most conventionally used classification of EVs based on biogenesis will be described here: apoptotic bodies, microvesicles, and exosomes, the generic term

"EVs" will be used in the discussions that follow as the biogenesis pathways of the analyzed particles cannot be confirmed in the present work.

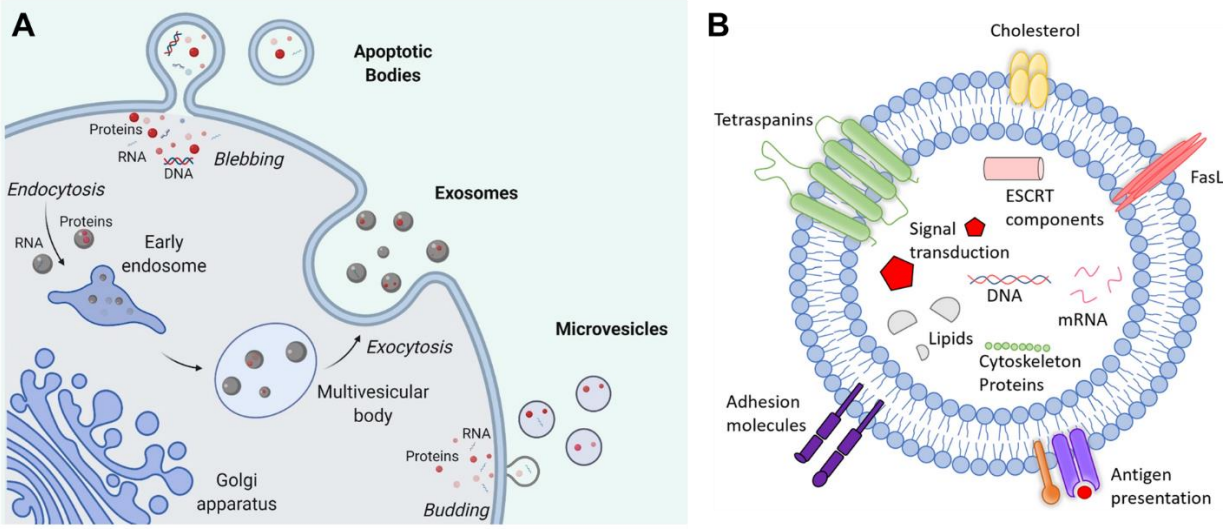

Figure 1. The biogenesis and composition of EVs. **A.** The biogenesis of EV subtypes: apoptotic bodies, microvesicles, and exosomes. Apoptotic bodies are generated when cells undergo apoptosis, microvesicles are formed by outward budding, and exosomes are released when multivesicular bodies fuse with the cell membrane via exocytosis[13]. **B.** The composition of EVs: EVs consist of lipids, nucleic acids, and proteins both within the plasma membrane and in the cytosol[14]. Figures reused from [6] and [7], licensed under CY BY 4.0 (https://creativecommons.org/licenses/by/4.0/)

Apoptotic bodies

Apoptotic bodies (ABs) are vesicles released by dying cells undergoing apoptotic cell clearance[15,16]. Apoptosis is essential for cells during embryonic development, growth, and normal maintenance of multicellular organisms and ensures the removal of aged and damaged cells from healthy tissues[17]. ABs range from 50 – 5000 nm in size and are formed during the separation of the cell's plasma membrane from the cytoskeleton due to increased hydrostatic pressure as the cell contracts[16,18]. The biogenesis of apoptotic bodies occurs in three stages: cell rounding, apoptotic membrane blebbing, and apoptopodia. Cell rounding describes dismantling of the cell performed mainly by caspases; cysteine proteases designed to cleave proteins. Proteolytic cleavage initiates

the dismantling of cell-cell adhesion complexes and cell-matrix focal adhesions[16,18]. Subsequently, an outward protrusion occurs that leads to plasma membrane (PM) blebbing and the formation of ABs[16,18]. ABs can contain fully intact organelles and therefore proteins associated with the mitochondria, nucleus, Golgi apparatus, and endoplasmic reticulum can be found in their cargo[19,20]. Relatively little is known about particular molecular compositions of ABs due to the diversity in apoptosis triggers and cell origins. Further characterization is needed to identify proteins and markers abundantly found in ABs.

Microvesicles

Microvesicles (MVs) are EVs ranging from 100 nm – 1000 nm in size and formed by ectocytocis, the direct outer pinching of the cell's plasma membrane[21]. The biogenesis of MVs consist of a series of lipid and protein activations and deactivations that lead to changes in membrane dynamics that facilitates membrane bleb formation. Ca^{2+} is first mobilized in the cell, initiating the deactivation of flippases and the activation of floppases, two lipid transporter proteins, and the activation of scramblases, which results in a loss of membrane asymmetry[15,22]. Calpain, a cysteine protease, then facilitates membrane bleb formation by disrupting the anchoring between the cell cytoskeleton and the membrane. Finally, contraction of the cytoskeletal structures by actin-myosin interactions leads to the outer pinching that forms MVs[22]. MVs largely contain proteins that cluster at the cell's plasma membrane as a result of their outward budding biogenesis pathway. Proteins markers commonly associated with MVs include tetraspanins, integrins, cytoskeletal proteins, and heat shock proteins; however, their proteomic profile can be highly dependent on the isolation method used due to the variability of size and density of the isolated MVs[23,24]. MVs have been found to be involved in cell-to-cell communication between local and distant cells, altering the

function of their recipient cells through the delivery of their cargo[25–27]. More recently, the role of atypically large MVs originating from cancer cells are found to be functionally distinct from other EVs and generally referred to as large oncosomes (LO)[8,28,29]. LOs are associated with abnormal assembly of molecular cargo and both structurally and morphologically unique[30]. In terms of abundance, they are far less abundant compared to smaller EVs and are difficult to purify accurately because of their large size[28]. As a result, the role of LOs has not been investigated in all tumor models yet.

Exosomes

Exosomes are EVs ranging from 30 – 150 nm in size and formed by an endosomal route, specifically through the inward budding of early endosome membranes[15]. Early endosomes themselves originate from the inward budding of the cell's plasma membrane and mature into multivesicular bodies (MVB) during the exosome biogenesis process[6]. As MVBs are fused with the plasma membrane, the exosomes are released into the extracellular space. Exosomes are bound by a single outer membrane and are also referred to as intraluminal vesicles (ILVs). During the budding process, cargo in the cytosol as well as transmembrane surface cargo are captured by the vesicle. Depending on the specific biogenesis pathway, the associated protein cargo can vary. MVBs and exosome release are regulated through the endosomal sorting complexes required for transport (ESCRT) pathway and can be categorized into two mechanisms: ESCRT dependent and ESCRT independent[18,27]. Exosomes formed and regulated by ESCRT dependent mechanisms rely on ESCRT proteins which are expected to be found in the exosome's cargo along with its accessory proteins, including Alix, TSG101, HSC70, and HSP90β)[15]. ESCRT is a molecular machinery consisting of ESCRT-0, I, II, and III, which sort ubiquitinylated proteins by working

sequentially[31,32]. Differing from the ESCRT-dependent pathway, exosomes formed and regulated by an ESCRT independent mechanism instead depend on the sphingomyelinase enzyme that converts sphingomyelin to ceramide[33,34]. Accumulation of ceramide then induces coalescence of the microdomain and triggers the formation of ILVs[33,34]. The resulting exosomes are often enriched with membrane proteins in the tetraspanin family, such as CD9, CD63, and CD81, and similar to MVs, exosomes play a role in cell-cell communication[8]. Additionally, exosomes participate in cell maintenance, tumor progression, and immune responses, leading to a growing interest in their use as biomarkers for disease, immunological applications, and drug delivery systems[23].

2.1.2. Tumor secreted EVs

EVs have been found to play a role in every stage of cancer biology, from promoting tumor growth and stimulating angiogenesis to generating the formation of pre-metastatic niches and promoting metastasis[8,35–37]. Tumor secreted EVs dictate communication between tumor cells and stromal cells in both the local and distant microenvironments and can redirect the function of their recipient cells through the delivery of their bioactive molecules.

The initiation and growth of tumors are not only regulated by tumor cells but also a variety of cells in the tumor microenvironment (TME) such as fibroblasts, endothelial cells, mesenchymal stem cells, and immune cells[38]. Tumor-secreted EVs are one of the main sources of communication between tumor cells and these neighbouring cells as well as the local microenvironment. These EVs can initially supress immune cells to decrease their proliferation and evade immune detection, either through the direct alteration of immune cell function or through indirect modification of

non-immune cells[39,40]. As a result, tumor secreted EVs influence non-cancerous cells to create a TME permissive to tumor growth and metastasis. One common characteristic of TMEs is hypoxia, the deprivation of oxygen in solid tumors due to inadequate blood supply and reduced microcirculation. In order for tumors to continue to grow despite hypoxic conditions, neo-angiogenesis, the process of new blood vessel growth, is required. Tumors are known to induce vascular growth and remodeling through the secretion of VEGF and PIGF growth factors, however, cancer EVs have recently emerged as being key mediators inducing pro-angiogenic responses[41,42]. Specifically, myeloma cells under hypoxic conditions have been found to secrete greater amounts of EVs containing the onco-micro-RNA miR-135b.[43] Endothelial cells receiving miR-135b containing EVs showed particularly accelerated angiogenesis ultimately as a response to hypoxia[43].

Although cancer cells are detrimental to their local TME, 90% of cancer related deaths are in fact due to metastasis of the primary tumor[44]. A number of cascading metastatic events occur before a tumor grows successfully in a secondary organ. The premetastatic niche (PME) can be defined as the progression of a location secondary to the primary tumor that is appropriate for the survival and proliferation of arriving circulating tumor cells (CTC)[45]. The secretion of EVs have been recently identified as an intracellular signaling mechanism that cancerous cells use to modify local microenvironments and distant organs to contribute to the formation of the PME. EVs play a wide role in the formation of the PME, including recruitment of cells to facilitate metastatic outgrowth and the modification of the metabolic environment[46]. As in the TME, tumor EVs' role in vascular remodeling through the delivery of miRNAs is a key step in PME formation. Presence of these miRNAs increases metastasis by facilitating the break down of endothelial cell barriers, allowing

cancer cells intravasate into the circulatory system and form metastatic lesions as they reach a secondary site[47]. Not only do EV miRNAs target endothelial cells, but the metabolic environment of the PME is also impacted. Recipient cells that take up miR-122 from tumor EVs were found to have reduced pyruvate kinase expression and decreased GLUT1 and glucose uptake[48]. This shows evidence that cancer cells can supress nutrient uptake by cells in secondary organs to renders the PME more nutrient rich for arriving tumor cells with high energy demands.

EVs as cancer biomarkers

Throughout the last decade, the role of liquid biopsies has been increasingly explored as a less invasive method for early cancer diagnosis. Patient samples from liquid biopsies, such as urine, saliva, and blood, can be abundant in biomarkers in the form of proteins, CTCs, platelets, and EVs. Among these, EVs have been shown to be one of the richest biomarkers as they are distributed throughout the body and their biological contents are well enclosed by a cellular membrane, allowing them to travel through the body's circulatory system and deliver their cargo to recipient cells[4]. Cancer cells have been recognized to produce many more EVs, and of altered composition, compared to healthy cells[49–51]. Such EVs have been found to be involved in numerous tumor processes, further supporting their potential to be promising candidates for cancer diagnostic biomarkers. Not only can these biomarkers be useful for disease diagnosis, but recent research has shown the potential of liquid biopsies to be used for dynamics and heterogeneity of tumors, as well as treatment resistance and monitoring. Several different EV biomarkers that have been identified to be associated with specific types of cancers are summarized in other reviews[3,5,52].

2.1.3. EV heterogeneity

One of the major challenges in the field of EV research is addressing heterogeneity within EV populations. Within a seemingly homogeneous population of EVs, evidence shows that a large degree of heterogeneity exists[6]. Populations of EVs are commonly purified and characterized into one of the aforementioned subtypes with isolation methods that are limited to size and density, such as ultracentrifugation and nanoparticle tracking analysis (NTA). However, physical and biological characteristics of EVs may not be correlated as EVs of similar size and density may be very distinct in terms of function. There is currently no method to isolate EVs based on biogenesis, which can cause significant overlap in EV subtypes and subpopulations.

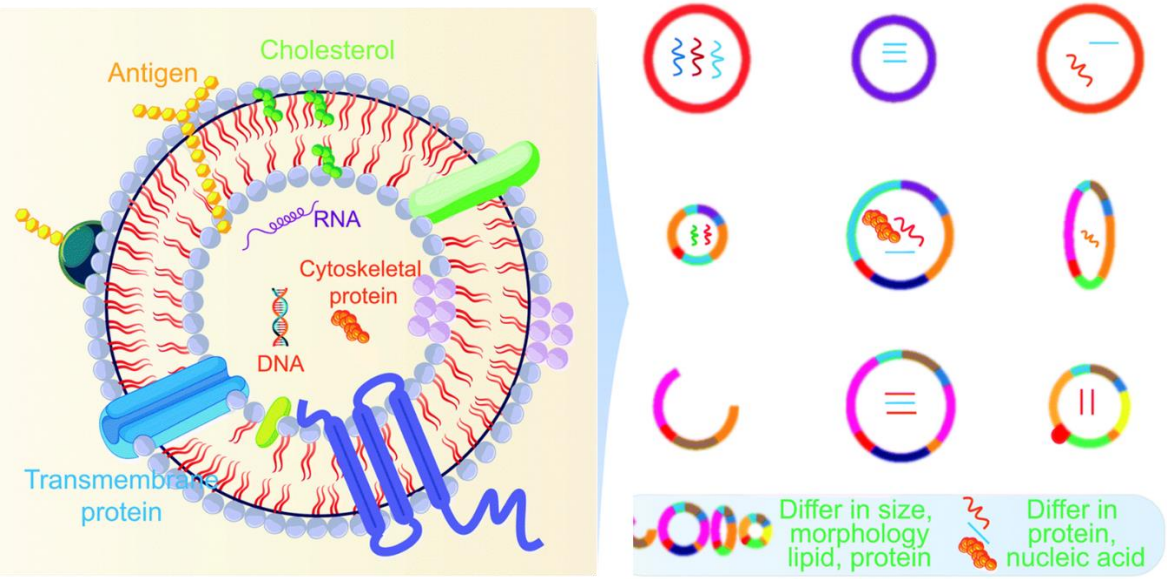

Figure 2. Extracellular vesicle composition and heterogeneity. EVs carry a variety of proteomic and genetic information, including proteins, lipids, and mRNA. Their physical characteristics (size, density, morphology), and cargo can vary substantially, resulting in heterogeneous EVs with different biological properties[53]. Figure adapted with permission of the Royal Society of Chemistry from [50]; permission conveyed through Copyright Clearance Center, Inc.

Beyond heterogeneity within an EV population, heterogeneity of individual EVs stemming from the same parent cell has been found to be unexpectedly high[53]. Uptake of cytosolic components

and packaging of EV cargo is reportedly a stochastic process, resulting in significantly different size, density, cargo, and composition of EVs secreted from even the same cell[53]. Therefore, EVs are said to represent a unique fingerprint of their parent cell. Moreover, EV heterogeneity arises as a result of physiological and pathological changes in the extracellular environment[54]. Cells are known to respond to external stimulus and changes in the form of modified EV secretions[8]. Modifications can consist of changes in the size and biogenesis of secreted particles, resulting in the secretion of a different subtype of EVs, but it can also involve changes in the cargo loaded in the EVs (Figure 2). Depending on the cell's physiological changes and pathophysiological conditions, the packaged cargo and membrane markers can vary greatly as the secreted EVs carry out specific biological functions[54]. As the EV cargo and composition can reflect what a cell's condition, EVs are a promising disease biomarker that can serve as a potential therapeutic tool. Isolating and characterizing distinct EV subpopulations can give insight into the state of parent cell and further uncovering EV heterogeneity and the role of subpopulations will advance the understanding of EV biology and their role in health and disease.

2.1.3.1. EV subpopulations

The heterogeneity among EVs could indicate that cells release EVs characterized by subpopulations with distinct composition or function. This suggests that subpopulations of EVs, beyond subtypes classified by size, with distinct cargo and membrane markers are released by cells to carry out specific biological functions. More recently, these subpopulations have been characterized based on the enrichment of certain protein markers, mainly tetraspanins and integrins. Tetraspanins are a class of surface proteins that transverse the EV membrane four times and contain four domains – N- and C-terminal cytoplasmic tails, a short and long extracellular

domain (ED)[55]. Tetraspanins are implicated in many cellular processes, such as cell signaling, fusion, adhesion, and regulation, and are generally said to have an important role as organizers of transmembrane and cytosolic proteins to create a multimolecular membrane network[56]. Because they have been found to be highly expressed in EVs, particularly CD63, CD9, and CD81, they are often used as specific EV markers[23]. Integrins are essential proteins involved in cell adhesion and extracellular matrix (ECM) attachment, and hence, favours long term interactions with cells targeted by specific EVs[57,58]. Integrins recognize proteins either on the surface of cells or in the ECM to mediate EVs binding to target cells and promote their fusion to deliver its molecular cargo[57,58]. Studies have illustrated that both tetraspanins and integrins found on EV membranes play a crucial role in guiding the targeting and selective uptake of EVs by recipient cells[59].

2.1.3.2. EV associated biomarkers

Identifying EV subpopulations in cancer cells can aid in characterizing disease and treatment states. Studies have demonstrated certain EV protein biomarkers can be reflective of both the tumors presence as well as cancer staging, highlighting the potential of tumor-derived EVs for cancer diagnosis and monitoring. In pancreatic cancer, EV expression levels of gyypican-1, a cell surface proteoglycan, was found to distinguish benign disease from early and late-stage cancer[60]. In metastatic melanoma patients, EVs were found to be presenting significantly higher expression of the proteins MDA-9 and GRP78, and thereby considered as potential biomarkers for the early detection metastasis[61]. Further analysis of melanoma patients identified TYRP-2, VLA-4, HSP70, and HSP90 as additional EV-associated protein biomarkers[62]. In breast cancer, a number of EV associated protein diagnostic biomarkers have been identified, including Del-1[63], CD47[64], HER2[65,66], EpCAM[65,66], and LDH-C4[67].

Furthermore, in metastatic cancers, tumor cells often metastasize to a specific organ and EVs have been found to play a role in this process, known as organotropism. Protein evidence linking EV subpopulations to biological functions of metastasis was identified by *Hoshino et al.* who found that certain integrin expression profiles of tumor EVs are associated with specific metastatic sites[68]. For example, EVs expressing the integrin ITG$\alpha_v\beta_5$ were found to bind specifically to Kupffer cells, mediating metastasis to the liver[68]. On the other hand, EVs expressing ITG$\alpha_6\beta_4$ and ITG$\alpha_6\beta_1$ bind specifically to lung-resident fibroblasts and epithelial cells, mediating metastasis to the lungs[68]. These findings suggest that tumor cells secrete subpopulations of EVs that express certain integrins that adhere selectively to different organs. Leveraging this, analysis of circulating tumor derived EVs may be useful for early detection of future metastasis.

2.2. EV analysis

EVs carry valuable cargo and are relatively new targets for bioassays, leading to many recent advances in the field of EV analysis. Although many techniques take advantage of physical characterization of EVs, purification and analysis of EVs based on protein enrichment provides much more relevant information as the transfer and detection of such proteins play a crucial role in cell communication[69]. As EVs carry these proteins from their cell of origin to recipient cells and are considerably stable biomolecules, EVs can mediate distant communication and modulate cell behaviors[69]. Furthermore, protein profiling of EVs, also referred to as EV proteomics, from healthy and diseased sources can help provide fingerprints for precision medicine. Analyzing EV proteomic signatures can uncover diverse signaling pathways, particularly in cancer where EV communication plays a role in many tumor processes[38,70–72].

Although there is no single standard method for quantitatively profiling EV proteins, mass spectrometry is the most widely used gold standard approach in proteomics[73]. Although MS is a powerful, high throughput technique able to identify multiple peptides in a single sample, it requires many preprocessing steps, and the sample is destroyed in the analysis process so it cannot be used for further downstream analyses[73,74]. To address these limitations, there have been great advances in the development of proteomic tools for measuring or profiling EVs from biofluids in the past decade.

2.2.1. Performance metrics of proteomic platforms

Sensitivity

The sensitivity of a method describes its ability to detect low concentrations of the analyte of interest and is often also related to as the limit of detection (LOD)[75]. In an assay, the sensitivity is typically the lowest concentration of signal that can be differentiated from the background[75]. In the context of EVs serving as diagnostic biomarkers for disease, a highly sensitive detection method is needed as acquiring large sample volumes is not always possible, especially in point-of-care (POC) testing. Although conventional EV analysis tools such as traditional enzyme linked immunosorbent assays (ELISA) and Western blot are well established and attractive for their ease of use and versatility, they are often limited by their poor sensitivity[76]. Several different aspects of a platform can be optimized to improve its sensitivity. For example, signal amplifications modifications can be employed to improve signal intensity[77], surface modifications can suppress nonspecific adsorption to reduce background signals or increase selectivity [78,79] or design modifications can be altered to increase binding probabilities[80]. Recent development of highly

sensitive EV analysis and visualization methods enable the resolution of EVs down to the single-particle level. Visualizing single-EVs will be discussed in later sections.

Multiplexing

The surface composition of EVs plays an important role in their biological function[23,81]. EVs are decorated with a variety of membrane proteins and may contain specific biomarkers to certain diseases[3,5,52]. However, evidence based on one single biomarker is insufficient to draw an appropriate conclusion or to clinically support a diagnosis for disease or treatment monitoring. For both research and POC applications, multiplexed screening to profile various biomarkers is highly valuable. The ability to quantitatively profile the surface proteins of EVs allows researchers to identify potential EV fingerprints associated with disease[3]. The additional advantage of multiplexing and running analyses in parallel is the reduced number of experiments and overall reduced sample consumption. This is key for POC applications where the biological sample may be limited. Another advantage of multiplexing is the ability to acquire a more biologically representative readout. Proteins carried by EV are important communication mediums between cells, therefore targeting multiple analytes at once is likely to reveal much more on EV-mediated interactions[82].

Multiplexed molecular profiling is typically enabled by the use of many fluorescent antibodies specific for many ubiquitous EV markers[83,84]. In both planar and bead-based arrays, proteins are captured onto the surface and secondary antibodies targeting specific proteins are then used to form a detectable immuo-sandwich complex. Ideally, using many different fluorescent secondary labels would enable the detection of many proteins in a single sample. However, the multiplexing

capability when using fluorescent probes in a single experiment is limited by spectral overlap between common dyes which becomes unavoidable beyond two or three colours due to limited spectral bandwidth available (~350 – 750 nm)[85]. This is relevant in both cytometry and optical readouts as spectral overlaps can lead to overestimations of protein expression. Multiplexed platforms interested in quantifying greater number of protein targets may choose to run the same sample on several parallel and imaged separately to avoid spectral overlap, but this requires larger sample volume and can present a greater variability between samples.

Temporal resolution

Cellular response to environmental perturbations often leads to dynamic changes in protein synthesis and degradation, ultimately resulting in changes in protein expression levels[86,87]. Secretion time course experiments monitor these cellular dynamics and determine secretion rates by collecting data in a time-dependent manner. The temporal resolution of such experiments can be described as the amount of time between measurements or imaging at the same location[88]. Methods with low temporal resolution are typically associated to studies interested in mapping the temporal proteome in terms of changing protein abundance, interactions, or localizations over the course of health and disease[89]. Low temporal resolution indicates that the number of time points assayed is limited, however, the data from a resultingly relatively longer-term study can identify key temporal changes and potential targets for disease monitoring and therapy. Higher temporal resolution is typically desired for monitoring dynamic secretion changes caused by an external stimulus[90,91]. Specifically in the context of EVs analysis, high temporal resolution analysis can answer the longing question of whether EV secretion rate of a cell is hereditary and whether the proteomic profile of secreted EVs vary with time of secretion. In the last several years, studies

interested in the dynamics of EV secretions have reported results with temporal resolutions ranging from minutes [90,91], hours[92,93], and days[94,95]. Real-time analysis of secretions describes measurements at the greatest temporal resolution. Otherwise, secretion rates can be normalized by back calculation, dividing the total secretions at a certain time point by the number of cells and time.

Spatial resolution

Here, spatial resolution refers to the measure of the smallest object that can be resolved by an imaging modality. This can be interpreted as the clarity of an image as low spatial resolution techniques are unable to differentiate between two objects that are relatively close together[96]. A method's spatial resolution often comes as a tradeoff to its multiplexing capabilities. For example, microarrays can perform a high degree of multiplexed phenotyping in a high-throughput manner but at a low spatial resolution[97,98]. Micro-sized spots of capture antibodies printed on a substrate to enrich specific EV subpopulations are subsequently probed with labeled detection antibodies for surface protein profiling. Spatial resolution on the EV level is limited by the size of the microspot as one spot captures around 25 000 EVs and the associated digital scanning technology is unable to resolve the signal beyond a single spot[97]. On the other hand, high spatial resolution techniques enable the visualization of EVs at the single particle level yet is only capable of a fraction of the multiplexing achievable by microarrays[99] . Such platforms are able to obtain much richer information, such as the heterogeneity of biomarker expression, the presence of EV subpopulations, and rates of EV secretion[99]. In the context of cancer EVs, resolution at the single EV level can enable the identification of tumor-derived EVs even in the presence of host cell-derived EVs. The increased spatial resolution is typically achieved by sensitive optical microscopy

combined with labeled techniques that rely on fluorescence or label-free techniques, such as interferometric scattering (iSCAT). These single vesicle analytical methods will be further discussed in detail in following sections.

2.2.2. Single EV proteomics

As previously mentioned, evidence shows that within a seemingly homogeneous population of EVs, a large degree of heterogeneity exists[6]. Individual EVs can differ in size, molecular composition, biogenesis, and function, all of which is masked in conventional methods that provide only pooled information about bulk population of EVs[100]. Due to this heterogeneity, there has been a growing effort to measure EVs with single particle resolution. Single EV analysis can be extremely valuable for studying tumor heterogeneity, rare tumor subtypes, and phenotypic changes that occur during therapy[53]. Several advanced analytical methods have been developed for characterizing the biological properties of individual EVs. Many recent technological advances have led to commercially available platforms for single EV analysis, including CytoFLEX and ExoView®, as well as novel tools for lab-based devices.

CytoFLEX

Conventional flow cytometers are widely used for quantitative and multiparametric single-particle analysis, their low detection sensitivity (> 300 nm) presents a challenge for analyzing EVs that may be as small as 50 nm[101]. High resolution flow cytometers and imaging flow cytometers were developed to overcome the sensitivity limitation of conventional cytometers, namely a semiconductor -based flow cytometer called CytoFLEX. CytoFLEX combines several innovations to maximize signal and minimize noise, ultimately enabling single particle detection down to 65 nm in size[102]. First, the use of silicone avalanche photodiodes (APD) with high quantum efficiency

and low electronic noise results in increased light-detection sensitivity[102]. Combined with low-power diodes, electronic and thermal noise is further reduced. CytoFLEX also takes advantage of a wavelength-division multiplexing (WDM) design that eliminates dichroic mirrors traditionally used in flow cytometers to divide light into colour bands within filter trees. Eliminating dichroic mirrors with WDM prevents 20-50% of signal[102]. Single EVs can also be immunophenotyped by labeling samples with detection antibodies prior to being introduced to CytoFLEX. With additional double and triple labeling, multiplexed co-expression analysis can be conducted[102,103].

ExoView®

The ExoView® platform from NanoView Biosciences is based on single-particle interferometric reflectance image sensing (SP-IRIS) coupled with immunofluorescence staining.

SP-IRIS relies on the interference of two reflected light paths, one of which passes through a bound particle, and another that passes through the empty part of the chip[104]. The interference pattern created as a result provides an increased resolution beyond the diffraction limit, enabling a particle detection limit down to 50 nm[104]. EVs expressing proteins of interest are captured by antibodies immobilized to specific microchips. The protein-capture oriented platform allows nearly true single event detection for the quantification and size analysis of small EVs. ExoView® is a robust and sensitive nanoparticle sensing assay, detecting single particles in samples with as few as 5 x 10^5 particles/mL. With the addition of fluorescent antibodies and overlaying images from fluorescence channels, quantitative information on co-expression of up to four markers per individual EV can be assessed. Valuable multi-phenotype information can be uncovered about an EV population with the ExoView® platform. Studies have reported the use of the ExoView® platform to characterize cell-specific EV populations based on their tetraspanins profiles[104,105].

Additional recent technological advances in the field of EV analysis have been in EV labeling, device development and high-resolution microscopy, allowing researchers to study the behavior of EVs at the single-vesicle level without such large and expensive commercial instruments[77,106–108]. With more accessible platforms for analyzing and visualize EVs a single-particle resolution, the complexity of EV biogenesis, cellular uptake, and secretion dynamics can be uncovered.

2.2.3. Optical methods for visualizing single EVs

Optical methods provide fundamental advantages that can address key challenges in studying EVs, including heterogeneity in EV populations, unknown sample concentrations, and correlating specific EVs to their origins. Although native EVs cannot be visualized by brightfield illumination due to their small size and the diffraction-limited capabilities of a microscope, attachment of a fluorophore which emits light enables the imaging of EVs by microscopy[109]. Rapid advances in fluorescent dye chemistries and labeling technologies provide unique opportunities for real-time, multiplexed rapid analyses otherwise not possible with non-optical techniques. Alternatively, label-free techniques that rely on light and optical properties to probe inherent features of EVs, such as interferometric scattering (iSCAT), are also being increasingly developed for single EV characterization. Other optical analytical approaches can enable the analysis of EVs in dynamic suspension with methods, such as nanoparticle tracking analysis (NTA) and flow cytometry, however, this section will focus on the analysis of EVs captured on a surface.

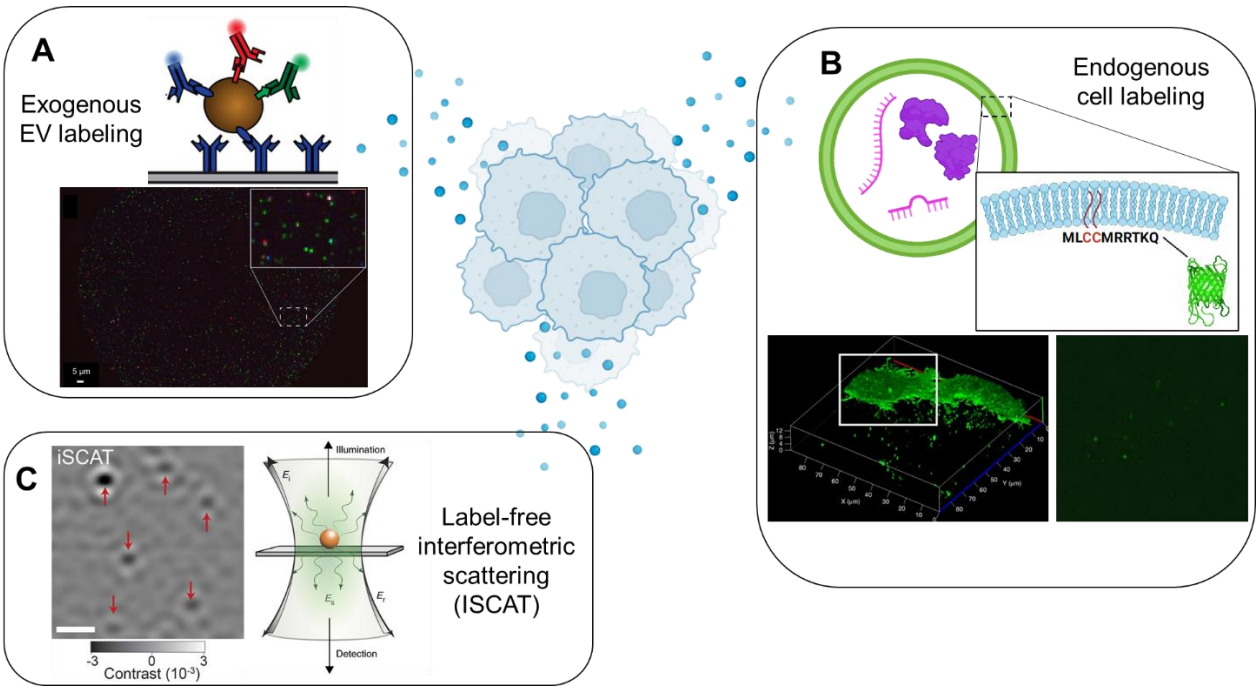

Figure 3. Overview of the main methods for visualizing single EVs discussed in this section. Schematic and data visualization using each technique are depicted. In the center of the figure, cancer cells releasing EVs is shown. **A.** Above: endogenous labeling of immunocaptured EVs with fluorescently labeled antibodies targeting membrane-expressed proteins. Below: multiplexed visualization of single EVs with fluorescence imaging[104]. Figures reused from [101], licensed under CY BY 4.0 (https://creativecommons.org/licenses/by/4.0/) **B.** Endogenous labeling of cells and their secreted EVs. Above: schematic diagram of EV membrane labeling with palmitoylated GFP (Palm-GFP) created with BioRender.com. Below: 3D reconstruction of confocal Z-stack images of a Palm-GFP-expressing 293T cells demonstrating EV release into surrounding regions[110]. Confocal microscopy of isolated single GFP-expressing EVs[110]. Figure reused from [107], licensed under CY BY 4.0 (https://creativecommons.org/licenses/by/4.0/) **C.** iSCAT, a label-free optical method for visualizing single EVs. Right: schematic demonstrating the operating principle of iSCAT detection[111]. The light reflected at the sample/glass interface is collected along with scattered light from the particle[111]. E_i, incident electric field; E_s, scattered electric field; E_r, reflected electric field. Left: iSCAT snapshot of single particles[112], scale bar: 1 µm. Figures in **C.** Adapted by permission from Springer Nature: Nature Protocols [50] Copyright 2016 and adapted with permission from [51]. Copyright 2018 American Chemical Society.

Exogenous EV labeling

The most widely used method for visualizing single EVs is with the use of exogenous labels, such as lipid dyes and conjugated antibodies (Figure 3A)[113]. Lipophilic dyes bind to the lipid bilayer membrane of EVs and exhibit a strong fluorescence signal[114]. DiR and DiD are commonly used

long chain diaklylcarbocyanines and diaklylaminostyryl dyes for EV labeling that emit fluorescence in the infrared region and have been reportedly used in EV biodistribution studies[115,116]. Other lipophilic dyes, such as PKH dyes use aliphatic tails to anchor on to phospholipid bilayers[113]. Although lipid dyes exhibit strong and stable fluorescence signals for ease of imaging, they present several challenges that must be considered. Lipid dyes have a long *in vivo* half-life that outlast EV degradation[117]. This can be misleading for long term studies as the dye remains long after EVs have degraded. Additionally, lipid dyes tend to aggregate and form micelles which can lead to false positive signals[114]. Another common organic dye for EV labeling is carboxyfluorescein diacetate succinimidyl ester (CFSE). CFSE is cell permeable and covalently binds to intracellular molecules through its succinimidyl group and is commonly used with flow cytometry[118,119]. CellTracker deep red (CTDR) performs similarly to CFSE with excitation and emission in the red region[120]. Most dyes can be added directly to cell media for ease of use and fluorescence imaging with good spatial resolution under optical microscopy.

EV-enriched surface proteins, most commonly tetraspanins CD9, CD81, and CD63 can also be targeted with fluorescently labeled antibodies to visualize EVs in both live and fixed cells (Figure 3A). Labeling with conjugated antibodies is commonly used in conjunction with high resolution optical techniques, such as total internal reflection fluorescence microscopy (TIRFM) and stochastic optical reconstruction microscopy (STORM) for imaging at the single-EV level. TIRFM and STORM imaging require EVs to be purified and immobilized, followed by an antibody incubation period and washing steps[90,107,121–123]. The resulting fluorescent EVs can be imaged with a resolution of 100 nm with TIRFM and 20 nm with STORM at a throughput of hundreds of EVs per image[107,123]. Labeling EVs with specific protein markers will however limit the EV detection

to certain subpopulations that express that marker[124]. To address this limitation, several platforms enable multiplex detection with the use of multiple fluorescently labeled antibodies, however, this is also limited by spectral overlap between common dyes and may require multiple rounds of labeling for higher multiplexing.

Endogenous cell labeling

A more general labeling strategy that aims to label all secreted EVs rather than a subpopulation expressing a certain marker is via endogenous cell labeling. This method modifies the cell's genetic material such that fluorescent proteins, such as GFP, are genetically fused with transmembrane proteins (Figure 3B)[125,126]. To track EV biogenesis, uptake, and dynamics, fluorescent proteins are typically fused with common endogenous EV membrane proteins, such as CD63 or CD9[124,126,127]. As EVs are derived from the cellular membrane, either through inward or outward budding, secreted EVs should also contain the fluorescent protein in their membranes[124]. Endogenous labeling therefore allows for direct visualization of cell secreted EVs with fluorescent proteins as reporters for EV imaging. Generally, plasmid DNA encoding the desired genetic sequence and cultured with the cells for transfection. To ensure stability of the cell line, the cells are often treated with drugs, such as puromycin, and considered to be stable when they are both fluorescent and drug resistant after long term culture[127]. However, genetically fusing fluorescent proteins to specific surface markers results in a fluorescence intensity that is dependent on the protein expression level and visualization is limited to certain subpopulation of EVs[120]. Alternatively, a more general labeling strategy tags the plasma membrane through S-Palmitoylation which enables labelling of a wider EV population. Lai et al. engineered a fluorescent EV labeling strategy based on S-Palmitoylation, a thiolester linkage between a cysteine

group and a fatty acid palmitic acid[124]. As cysteine groups are found on proteins and palmitic acid in the cellular membrane, S-Palmitoylation enables the association of a fluorescent protein to the cell membrane for whole cell labeling and live-cell visualization. Still, endogenous labeling presents several challenges as steric hindrance of the genetically modified associated protein could affect EV cargo content and uptake[120]. Additionally, labeling efficiency can vary and is difficult to characterize. However, overall genetic labeling is more stable compared to fluorescence reporters, it is compatible with living cells, and most notably, it enables real-time monitoring of EVs.

Interferometric scattering

Interferometric scattering (iSCAT) is a label-free microscopy technique able to sense single particles by detecting the amount of light the particle scatters as it binds to a surface[128,129]. Single particle detection is achievable as iSCAT microscopy amplifies the weak scattered light by a single particle by interferometric mixing with a secondary reference wave (Figure 3C)[130]. The amount of scattered light is proportional with its polarizability, therefore, assuming the particles have a similar refractive index, the measured scattering signal can be correlated to the size of the particle[130]. The iSCAT microscope can be built by modifying an inverted microscope setup[111,112]. A beam splitter is added between the laser and the objective which transmits the incidence beam and reflects the reference and scattered beams at 90° to the incident beam. In this set up, a laser beam is focused to the back focal plane of an objective with a high numeral aperture, creating a plane wave at the objective's forward focus. The beam is directed to the sample in an aqueous solution through a glass coverslip. The plane wave reflected at the liquid-glass interface is then collected back through the objective, split at the beam splitter, and recollimated into the camera

for detection. When a particle is captured onto the glass surface, light is scattered by the particle and the spherical wave it produces is also collected through the objective and focused in the camera[112]. When the reference beam is superimposed with the image of the scattered field, the scattered and reference beams interfere, and the detected particles appear as diffraction-limited dark spots. As iSCAT is a label-free microscopy method that does not rely on any secondary reagents or fluorescent probes, iSCAT can be a valuable tool for studying dynamics of cell secretions with subsecond temporal resolution[131].

2.3. Single cell analysis

Cell to cell variation is a well-established characteristic of multi-cellular organisms. Among a seemingly homogeneous population of cells, individual cells can be unique and behave differently from one another (Figure 4)[132–134]. Conventional studies of cell behavior in response to perturbations are obtained from bulk assays on a population of many cells. These assays cannot capture responses of individual cells, who's behavior may not reflect those deducted from the bulk due to ensemble averaging[135]. In the context of cancer, intratumoral heterogeneity is directly observable in cell subpopulations harbouring unique genetic profiles and molecular signatures for distinct biological functions[136]. Within the same tumor, certain subpopulations may dominate the tumor composition, however, minor subpopulations can determine the progression and recurrence of the disease[137]. This phenotypic heterogeneity has greatly stimulated the advancement of analyses at the single cell resolution necessary for identifying the underlying complexity of cells in health and disease.

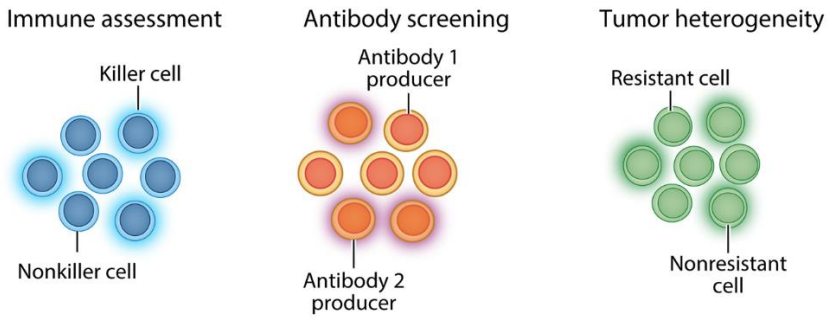

Figure 4. Biological implications and applications of single cell analyses. For example, measurements from individual cells can enable identification of immune cell types, achieve antibody screening, and assess of cancer cell heterogeneity[138]. Figure adapted with permission from Annual Reviews, Inc. from [7] conveyed through Copyright Clearance Center, Inc.

2.3.1. Single cell proteomics

Proteins provide essential details about a cell's activity and structure, making proteomics and its adaptation to single-cell systems a high priority in recent research[139]. Proteomics has however been one of the most challenging aspects in single-cell studies for several reasons. Unlike genomics and transcriptomics, there is no amplification process available in proteomics as proteins are either detected directly based on its amino acid sequence or indirectly by detecting the presence of an affinity binder bound to the protein of interest [140]. Sensitivity is of great importance to single cell protein characterization as protein abundance can vary greatly across the proteome of a single cell, with many found in low abundance[141]. Designing instruments and assays with sufficient sensitivity has been a key barrier to the widespread adaptation of single cell proteomics as the method must be sensitive enough to collect native data from a single cell. Specifically, methods that rely on affinity binders, such as antibodies, to detect select protein epitopes often struggle because many antibodies have low specificity for their targets, resulting in nonspecific protein detection[142]. Despite developments in recent years, current methods still suffer from low sensitivity and low throughput as single cell secretion samples are typically small in volume to reduce the loss of

proteins and limit the dilution of lower abundance secretions attributed to single cell[140]. But due to their small volume, conventional methods, such as mass spectrometry, often pool secreted protein samples across single cells to achieve protein quantification[143]. Although pooled samples achieve higher protein abundance signals, secretions cannot be traced back to their cell of origin even though secretions were collected from single cells. Furthermore, temporal resolution is greatly reduced, and secretion dynamics cannot be unraveled.

Single cell protein analysis also has the added challenge of single-cell separation and capture methods, prior to cell treatment and subsequent protein quantification. Individual cells must be laboriously isolated and retrieved intact so that no material is lost. Cells must also be viable throughout, creating more time and handling constraints in sample preparation. Single cell separation strategies include cell sorting by microarrays, microfluidic devices, and droplet-based methods. These methods often require more careful handling and control of small volumes for rapid transport and accurate positioning of cells[139]. Another consideration is that most single cell analytical methods remove cells from their tissue context, however, where a cell resides impacts their behavior[144]. By disaggregating cells, researchers lose the way cells behave in the natural complex environments, surrounded by ECM and neighboring cells[144]. Combined with low specificity and limited throughput, current generation of single-cell protein analytical methods face many challenges for understanding the interactions and functions of proteins at single-cell resolution[143]. Yet, over the last several decades, numerous platforms have been developed in attempt to present solutions to these challenges and further advance the landscape of single-cell protein analysis (Figure 5).

2.3.2. Platforms for single-cell proteomic analysis

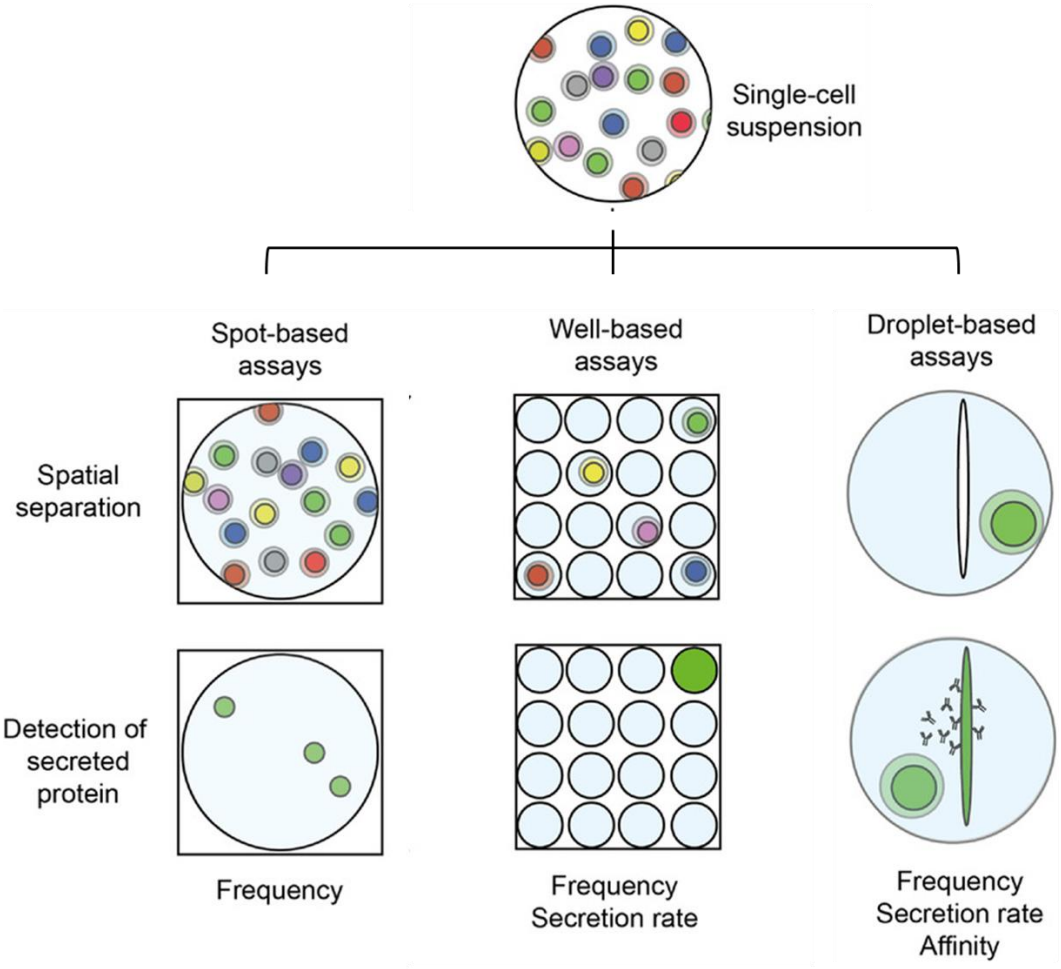

Figure 5. Schematic representation of different technologies enabling analysis of protein secretions at the single cell level that are discussed in this review[132]. The described technologies all rely on spatial separation of individual cells and labeled reporters, however, differ in terms of read-out, multiplexing potential, throughput and resolution. Spot-based assays such as the ELISpot are based on seeding cells on a protein-binding membrane and enable simple determination of the frequency of secreting cells. Well-based assays encapsulate cells in individual small volume wells for accurate and rapid quantification of secretions. Droplet-based microfluidic assays encapsulate individual cells in an emulsion for surface-free high-throughput detection. Figure adapted from [129] licensed under CY BY 4.0 (https://creativecommons.org/licenses/by/4.0/)

Enzyme-linked immunospot (ELISpot)

The ELISpot assay is an adaptation of classic immunosandwich assays and is one of the most conventional platforms for single cell secretomic studies[145]. In an ELISpot assay, cells are first

placed into an antibody coated well and incubated as it secretes antigens that are captured by the immobilized antibodies. After the desired incubation period, the cell is washed away and the well is incubated with biotinylated detection antibodies followed by streptavidin conjugated to fluorescent substrate. Affinity between the biotinylated antibody and the streptavidin-fluorescent substrate results in a coloured spot, where each spot describes the secretions of a single cell. Analysis of individual spots ultimately allows for comparison and differentiation between the secretions of various single cells[145].

Readout of the assay is based on analysis of the fluorescence intensity and size of the spots to determine and compare the relative frequency of secreting cells[146]. To run a successful assay, the concentration of cells seeded into each well must first be optimized to avoid overlapping spots that mask individual cell secretions, while ensuring enough spots are produced for statistical significance[132]. However, even with an optimal concentration of cells seeded, readout is often an underestimate since the surface will not capture all secreted molecules and only a subset of cells secrete at a high enough level to produce a resolvable spot[147]. Additionally, as the captured secretions are labeled for analysis after a set incubation period, the readout is done at a single timepoint which masks any dynamic changes due to cell communication or changes in cell environment. Another limitation of the ELISpot is that the secretions cannot be traced back to specific individual cells because the cells are washed away prior to fluorescent labeling and visualization. Although unique secretions can be identified, further data obtained from the assay is limited as additional studies cannot be conducted on cells that produced those specific secretions. Finally, commercial ELISpot wells are often only coated with one or two types of detection antibody, thus limiting multiplexed proteomic analyses[146,148]. The ELISpot derivative, the

FluoroSpot, was then developed to increase the multiplexing capability up to four targets by using fluorochrome-conjugated detection antibodies[149,150].

Microwell arrays

Conventional well plate assays require large volumes of reagents and long incubation times to allow for diffusion of secretions and detection antibodies to the surface[132]. Recently engineered microwell arrays greatly reduces the dimensions of individual wells to tens of micrometers, resulting in nanoliter or even picoliter volumes in each well[151,152]. This allows secreted molecules to be captured much quicker and be more concentrated within the well. As the sensitivity in antibody-based assays relies on analyte concentration rather than number of analytes, the nanoliter-sized wells concentrate analytes more effectively and increase the overall sensitivity of the assay[153]. Microwells are also able to achieve single cell resolution as cells compartmentalized and isolated from neighboring cells. Potential interactions between cells are avoided and secretions from individual cells can be analyzed without cross contamination of secretions from surrounding cells. Furthermore, the secreted EVs can be traced back to their cell of origin to identify unique single cells and be recovered for additional downstream analysis. One chip can contain an array of thousands of individual microwells, allowing for a much higher throughput compared to traditional well-based assays[154,155]. To load the wells with cells, a cell suspension is often introduced to the surface and cells are left to sediment passively or actively with centrifugation[132]. Loading efficiency can be optimized by modifying well diameter or by adjusting the cell suspension concentration[156]. Single cell loading can be challenging as the proportion of wells that are loading with a single cell rather than multiple cells is dictated by Poisson statistics[157]. With Poisson statistics, the concentration of cells that maximizes the loading of exactly one cell per well is

determined, however, the majority of wells will contain no cells or multiple cells[157]. For a single cell experiment in an array of thousands of wells, the user can choose to only look at wells where a single cell was loaded.

For single cell proteomic analyses, microwell array chips are often coupled with a glass surface coated with capture antibodies[94,158–160]. As EVs are secreted by the cell, they diffuse across the microwell and are captured by antibodies immobilized on the surface. Following the desired incubation period, the chip can be separated, and the glass surface is incubated with detection antibodies, often fluorescently labeled. Quantitative data is obtained from the readout by comparing the fluorescence intensity of each well to a calibration curve[94,158]. However, as fluorescent labeling occurs at a single time point, current microwell arrays are not suitable for dynamic analyses of cell secretions. As previously mentioned, one of the main advantages of microwell arrays is its ability to recover cells for subsequent studies. Cells identified as rare or diseased can be further analyzed by different methods, such as single-cell RNA sequencing, to get a deeper understanding of cell heterogeneity[92].

Microfluidics

Microfluidics takes advantage of the behavior and manipulation of minute volumes of fluid[161,162]. Contrary to fluids moving through large channels that mix convectively, fluid streams in microfluidic channels exhibit laminar flow characterized by a low Reynolds number[162]. In a laminar flow system, multiple fluids can flow in parallel with mixing only occurring as a result of the diffusion of molecules across the interface between fluids[162]. This is an attractive property as it enables the precise manipulation of fluids to perform relatively complex assays in addition to

reduced amounts of reagents and sample volumes. Single cell systems can take advantage of such fluid manipulation with a particular branch of microfluidics, known as droplet microfluidics, where individual cells and their secretions are isolated in precise volumes and analyzed in a high throughput manner[134]. Similar to microwell assays, cells are compartmentalized in individual droplets. Droplets are formed in microfluidic devices using two immiscible fluids to create an emulsion that encapsulates single cells in picoliter sized droplets. Most commonly, an aqueous fluid is used for the inner phase and encapsulated in an inert oil[132]. Similar to microwell arrays, single cell loading relies on Poisson statistics where the concentration of cells can be optimized to maximize the encapsulation of individual cells, but the majority of droplets will contain zero or multiple cells[157]. However, because droplet analysis has very high throughput, hundreds of thousands of cells can still be analyzed in each experiment[163]. Furthermore, cells, reagents, antibody modified beads, fluorescently labeled secondary antibodies, can all be encapsulated together to conduct complete experiments within a single droplet[164]. Readout for droplet microfluidic experiments is typically achieved by fluorescence detection where the droplets pass through a laser to measure fluorescence, similar to flow cytometry[77,134,164]. Incubation time is thus a critical parameter that must be optimized as the binding of the detection antibody to the secretions must occur before the droplet reaches the laser. As this is measurement occurs at a final time point, the dynamics and patterns of cell secretions cannot be resolved with droplet microfluidics.

2.4. Single cell EV analysis

Single cell analyses have shown that cells secrete unique EV subpopulations characterized by different membrane protein expression[92–94,122,158]. Since cell secretions are mediators of cell signaling and the expression level of proteins on EVs can be tightly controlled in a biological

system, single cell EV analysis can give an insight into an individual cell's physiological and pathological conditions[10,11]. Further, as EVs contain biological cargo and membrane protein markers stemming from their cell of origin, EVs are said to represent a fingerprint of their parent cell, thereby indicating the parent cell's physiological and pathological conditions[2]. Probing EVs at the single cell level is thus crucial to uncovering EV heterogeneity that is often hidden in larger cell populations[94,122]. Single cell EV analysis first requires the isolation of single cells from larger populations, followed by methods to capture secreted EVs and finally a highly sensitive detection method. By analyzing isolated single cells, EV biogenesis and secretion can be studied without any potential interaction with other cells. Ultimately, cell to cell paracrine communication through EV signaling can be assessed.

2.4.1. Platforms for studying EV populations from single cells

Several platforms have been developed in the past several years for the detection of EVs at the single-cell level, most of which use microwell array chip formats. *Cai et al*. developed the Transolcation Secretion Assay (TransSeA)[92], an open platform for parallel single cell EV analysis (Figure 6A). TransSeA features an open design for facilitating media change and modifications of microenvironments, and technology for locating and tracking single cell secretions to enable correlation studies between secretion patterns and cell phenotypes. Single cells are positioned in a PDMS through hole layer attached to a polyester thin film with 0.8 μm pores to allow the passing of cell secretions while confining the cells. Secretions are then collected on one of two assay bases, one that is target specific and one that is holistic. The target specific assay is an antibody coated glass plate that immobilizes secreted EVs and is labeled with biotinylated detection antibodies followed by streptavidin-conjugated quantum dots for analysis. For holistic collection, the

secretions can be drained into an uncoated microwell and later analyzed by droplet digital PCR. TranSeA was used to study cell EV secretion rates over a 3 h collection period and found distinct differences between genetically identical single cells. The TranSeA targeted assay was however only a single-plex assay looking at CD63-positive EVs, limiting secretion analysis to one EV subpopulation.

Ji et al., demonstrated a microchip platform for multiplexed profiling of single-cell EV secretions using antibody barcodes[158] (Figure 6B). Their platform combines a high-density microchamber array to a spatially resolved antibody barcode glass slide to realize multiplexed detection. Single cells are isolated in the microchambers and concentrates the secreted EVs in just nanoliters of volume. The antibody barcode accommodates up to nine different antibodies used to form detectable immune-sandwiches for EV detection. The two surfaces are clamped together to trap the single cells and imaged to record cell positions. After an overnight incubation, the surfaces are separated, and the glass slide is incubated with a cocktail of detection antibodies for detection. Fluorescent positive spots intersecting antibody barcodes demonstrate the presence of EVs with different surface proteins secreted from the same single cell. The platform was successfully applied to the analysis of human oral squamous cell carcinoma (OSCC) cells to reveal secretion heterogeneities, in particular, observing that the expression of certain EV subpopulations decreased in metastatic tumor cells and the profiling EV secretions from the same single cells.

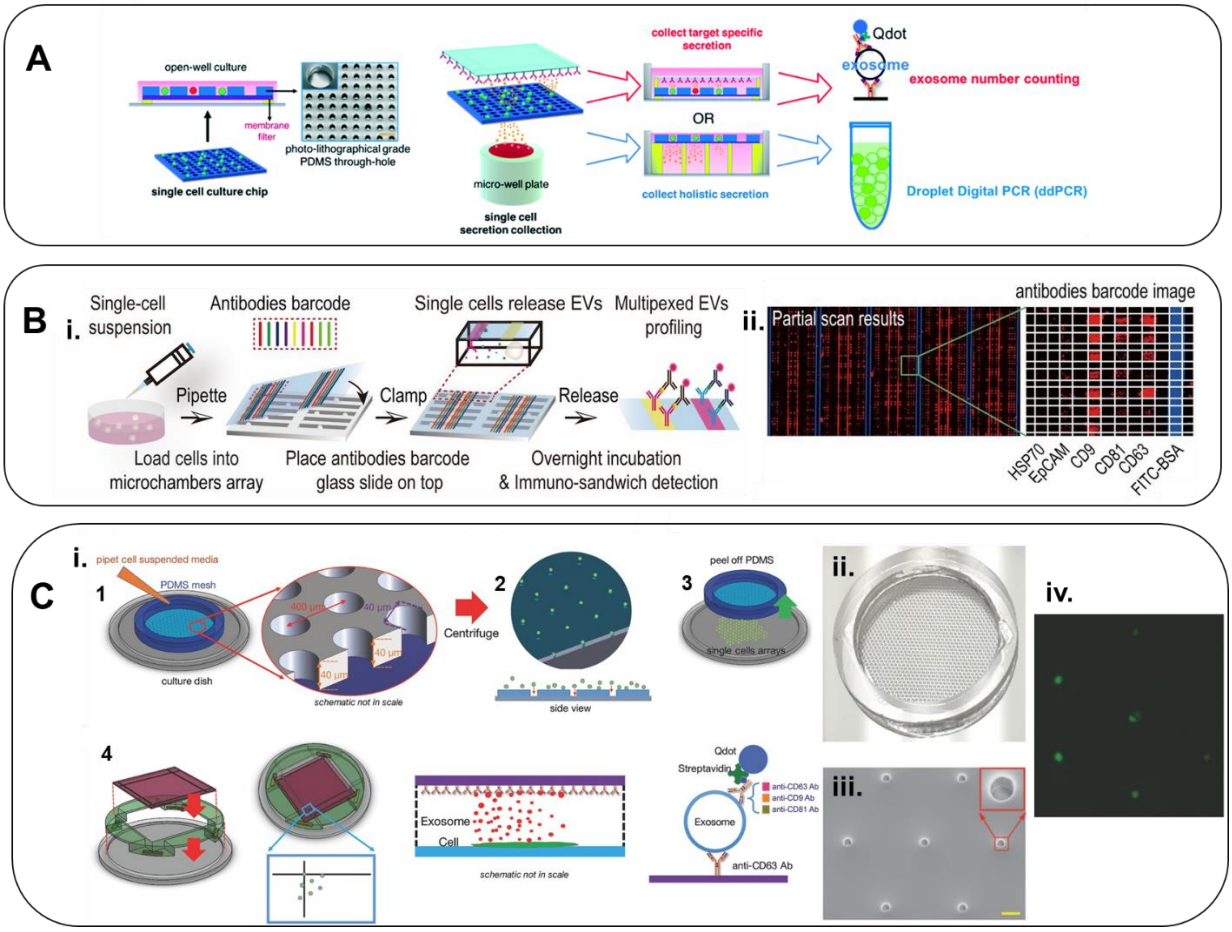

Figure 6. Schematics and images demonstrating recently developed platforms for single cell EV detection. **A.** The TransSeA platform enabling single cell culture and single cell secretion harvesting, either target specifically with an antibody functionalized plate for EV quantification or holistically for droplet digital PCR[92]. Figure used with permission of Royal Society of Chemistry from [31]; permission conveyed through Copyright Clearance Center, Inc. **B. i.** A platform for the multiplexed profiling of single-cell EV secretion that combines a microchamber array and a spatially resolved antibody barcode glass slide[158]. **ii.** Representative fluorescence detection images (partial and enlarged) showing data obtained from multiplexed single cell EV profiling. Figure adapted from [27] with permission. **C. i.** Preparation and operation of single cell assay for analyzing EV secretions[93]. The cell secreted EVs are collected on a functionalized cover glass and labeled with quantum dots to become fluorescently visible. **ii.** Photograph of the PDMS mesh supported by a PDMS ring. **iii.** SEM micrograph of PDMS mesh with through holes for cell loading. Scale bar is 100 µm. **iv.** Fluorescence image of loaded single cells spatially separated by loading with the PDMS mesh. Figure used with permission of John Wiley and Sons from [38]; permission conveyed through Copyright Clearance Center, Inc.

One single cell assay for the study of EV secretions that did not use spatial confinements to isolate cells was the platform developed by *Chiu et al*. (Figure 6C)[93]. Here, single cells were pattered as

an array onto a glass surface using a temporary PDMS mesh to allow single-cell culturing without space restrictions. A second surface functionalized glass slide was placed 100 µm above the cell surface with the use of a support frame. The surface-treated glass slide collects EVs as they are secreted by the single cell. In a time course experiment, surface-treated glass slide captured EVs at certain time points which were then labeled with biotinylated antibodies and subsequently bonded to streptavidin conjugated quantum dots. The quantum dots were visualized by fluorescence microscopy and counted over each area corresponding to the location of a single cell to investigate the properties of secreted EVs by a single cell. Time-lapsed observations were made of single cells every 24 h over four days to derive single cell EV secretion rates. *Chiu et al.* demonstrated that their platform can be used to study the effects of drug treatment on different cancer cells by presenting treatments to the cells and studying the associated EV secretion rates by individual cells.

2.4.2. Combining single cell and single EV detection

This push is for single EV analysis is analogous to the development of single cell analysis that has driven the EV field in the past several years. A major challenge in the use of EVs as a source of biomarker for cancer diagnosis is the high variability of EVs secreted by individual cells due to the stochastic nature of EV biogenesis and release[165]. Purified EVs from liquid biopsy contains a mixture of EVs secreted by cells all throughout the body. The bulk analysis makes it is difficult to correlate specific EVs to their parent cells thereby identifying which EVs are secreted by tumor cells, and which are secreted by healthy cells[166,167]. As the combination of an EVs membrane proteins and biological cargo can differ substantially between EVs, heterogeneity exists even between EVs stemming from the same parent cell[7,8,168,169]. To truly uncover EV heterogeneity,

novel methods are needed to analyze EVs at the single particle level from the same parent cell without potential interaction with other cells.

Of date, the only work reporting the analysis of single EVs directly from single cells was a platform developed by *Nikoloff et al*[122]. Their platform combines a microfluidic device containing isolated chambers with a multicolour TIRFM imaging platform for robust capturing, quantifying, and phenotypically classifying single cell secreted EVs at the single particle level (Figure 7). In their setup, cell suspension solution is flowed through the microfluidic device and single cells are hydrodynamically trapped by chambers enclosed by pneumatically controlled concentric valves. The region around the chamber surrounded by a second set of pneumatic valves and coated with antibodies targeting EV associated proteins to isolate and immobilize EVs secreted by the cell over the experimental period. Taking advantage of the microfluidic flow through system, fluorescently labeled antibodies can then be supplied to the captured EVs for imaging by four-colour TIRFM. TIRFM provided high optical sensitivity and spatial resolution to enable phenotypic-specific multiplexed classification of single EVs. In turn, this enabled the ability to track phenotypic variations between EVs secreted from single cells. Using antibodies targeting against four different protein markers, the distribution of EVs positive for only one, two, three, and all four markers outlines the heterogeneity of cell secretions and supported the hypothesis that subpopulations are secreted at different frequencies. Their system was then used to quantify the down-regulation of EV secretion by supplying cells with an enzymatic inhibitor. A general down-regulation in EV secretion was observed but few subpopulations were more strongly affected, indicating a nonhomogeneous effect on EV subpopulations. However, the platform did not operate without flaws as unspecific background adsorption was a notable issue, with 26% of unoccupied wells

showing positive EV signals. Moreover, constraints were observed in TIRFM imaging sensitivity as some EV populations that tested positive for certain markers did not appear above the signal detection threshold in their fluorescence channels. Although the platform had inherent limitations, this was the first demonstration of robust counting and classification of single EVs truly secreted by single cells.

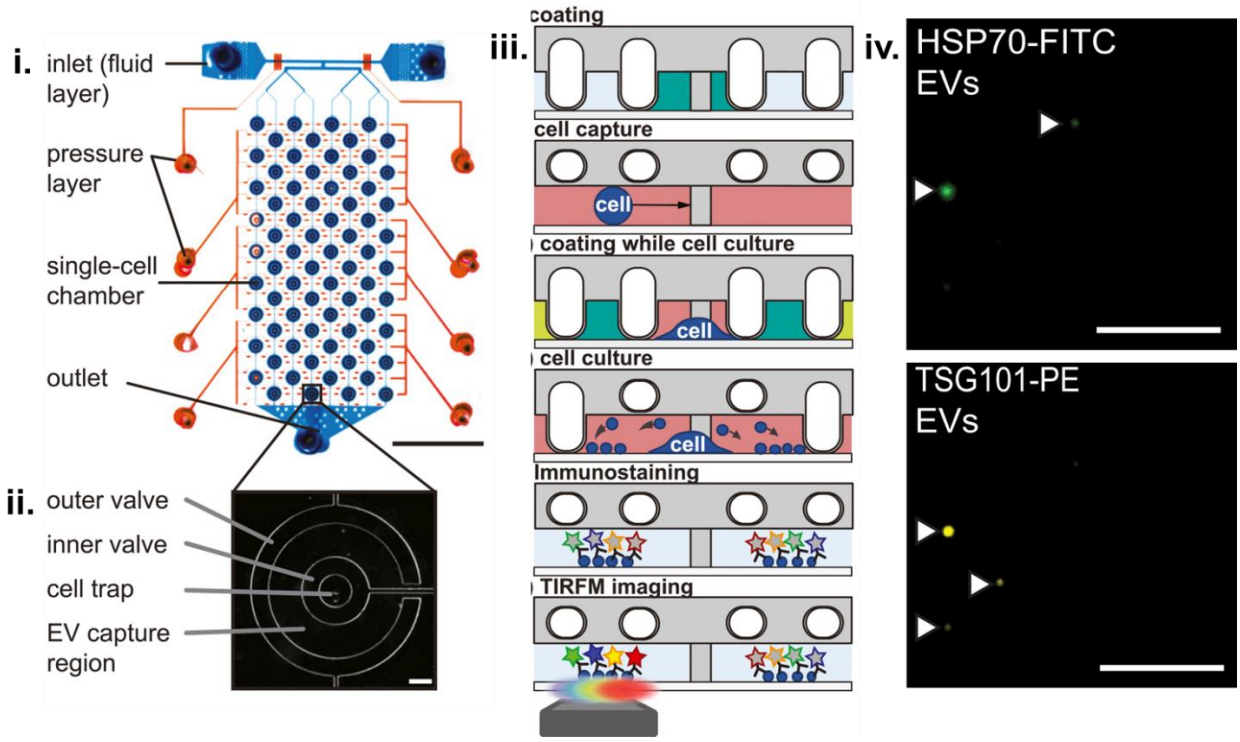

Figure 7. The *Nikoloff et al.,* platform for studying single EVs secreted directly from isolated single cells. **i.** Schematic showing the experimental approach of the PDMS microfluidic device in blue combined with the pneumatic control layer in red. **ii.** Image of a single culture well where the outer valves encloses the EV immobilization area and the inner valve physically isolates the single cell. **iii.** Schematic demonstration the assay operation. The surface is functionalized with biotinylated BSA, NeutrAvidin, and biotinylated antibodies to immobilize secreted EVs. The EVs are then labeled with fluorescent-conjugated antibodies and imaged by TIRFM. **iv.** TIRFM images of immobilized EVs after 24 h of incubation from MCF-7 cells labeled with HSP70-FITC, green (top) and TSG101-PE, yellow (bottom). Figure adapted from [119] licensed under CY BY 4.0 (https://creativecommons.org/licenses/by/4.0/)

Studying single EVs secreted directly from single cells is further motivated by interests in studying secretion dynamics. Secretion dynamics describes the time and rate of cell secretions[112]. All cells

secrete proteins and other biomolecules, but some cell types with regular secretion patterns have been found to secrete through different pathways when triggered an external stimulus[170]. The immune system is a well-known example of this as paracrine signaling by cytokine secretion is suggested to be a highly coordinated response[171]. Since EVs are also mediators of cell-to-cell communication, external stimulus may trigger similar secretion patterns to initiate a desired response. External stimulus could include hypoxia due to the tumor microenvironment or drug treatment targeting tumor cells[172,173]. By analyzing the secretion dynamics of tumor cells, we can gain a better understanding of the role of EVs in tumor progression, develop diagnostic standards, and monitor the effects of cancer treatments.

2.5. Project Rationale

The analysis of single EVs secreted from single cells was previously explored in a microfluidic device using pneumatic valves to isolate cells and their secreted EVs and classified EVs by immunostaining[122]. While this platform established the feasibility of single cell, single EV measurements, experiments were limited in time resolution due to single timepoint fluorescence labeling for EV visualization. Lack of temporal resolution is seen across other EV analysis platforms as well, and as a result, little is known about how EV secretion abundances are affected by biological or external processes or whether the secretion rate is representative of a cell's physiological and pathological state[174]. Without the ability to capture short-term responses, we have a limited understanding of EV secretion dynamics. We have therefore identified a need to develop a single cell, single EV platform that provides a robust means to characterize secretion dynamics and EV heterogeneity. The resulting platform can be leveraged to evaluate time coursed

EV secretion dynamics, identify conditions that enhance or inhibit EV secretion, and further understand cellular communication between cancer cells.

The proposed platforms will meet the following requirements: (i) isolation of single cells, (ii) isolation of cell secreted EVs, (iii) media exchange to maintain cell viability, (iv) imaging at the single EV resolution, and (v) time course imaging. A number of design elements will be incorporated for the isolation of single cells and their secreted EVs. In order to capture such short-term responses of EV secretion, we will employ endogenously fluorescently labeled cells that secreted labeled EVs. As a result, the secreted fluorescent EVs can be directly visualized, and high temporal resolution can be achieved beyond the means of traditional fluorescent labeling. Here, two proposed platforms will be discussed for their suitability for time course analysis of single EVs secreted by single cells. The first platform consists of a hydrogel microwell array (HMA) based on compartmentalization of single cells and the second is a simplified shallow flow cell (SFC) based on spatial isolation of single cells. Strengths and weaknesses of each platform will be discussed, followed by validation and proof of concept experiments of EV detection using the SFC platform.

3. Materials and Methods

3.1. Resin and prepolymer solution preparation

Commercial MiiCraft BV-002a black resin (Creative CADworks) was used for 3D printing molds for casting. Low molecular weight (LMW) poly(ethylene glycol) diacrylate (PEGDA) (average molecular weight 250, Sigma-Aldrich) resin was prepared with an in-house formulation. High molecular weight (HMW) PEGDA prepolymer solution was also prepared in-house as a mixture of 4% PEGDA (average molecular weight 6000, Sigma-Aldrich), 10% hydroxypropyl acrylate (HPA) (Sigma-Aldrich, 95%), and 1% lithium phenyl-2,4,6-trimethylbenzoylphosphinate (LAP) photoinitiator (Sigma-Aldrich, >95%). LAP was dissolved at a concentration of 3% (w/v) in water and added at a concentration of 1% (v/v) to the prepolymer solution. All resins mixtures were stirred on a stir plate and stored in amber glass jars.

3.2. 3D printing parameters and post processing

A master positive mold of the microwell array platform was 3D printed with the Tiger Apex 4K XHD PRO optical 3D printer. Molds were printed with 20 µm layer thickness with a curing time of 1.60 s. Molds were washed in an isopropanol (IPA) bath on a shaker for 30 min after printing and post-UV cured for one minute twice, rotating the print 90°C in between, to remove and cure any excess resin. Finally, the molds were baked in a 60°C oven overnight and stored at room temperature until use.

3.3. Hydrogel microwells fabrication and characterization

3.3.1. Vacuum assisted hydrogel loading

Polydimethylsiloxane (PDMS) base (Sylgard 184, Dow Corning) and curing agent were mixed at a 10:1 ratio and degassed in a vacuum desiccator. The PDMS mixture was then cast over the 3D printed positive molds and cured in a 60°C oven overnight. The resulting PDMS negative molds were cleaned by sonication in 100% ethanol for 5 min then washing with water and dried with nitrogen gas. A single inlet hole was punched at the main channel with a 0.5 mm punch. A 1.5 x 1.5 mm piece of 3D printed LMW PEGDA was used as the base of the platform. An enclosed mold was then assembled by placing the replicated PDMS negative on the LMW PEGDA to seal the areas around the microwells and the channels. To fill the mold, HMW PEGDA prepolymer solution was applied as a droplet at the inlet. Vacuum was applied to degas the air in the gap, followed by re-pressurization of the system to drive the prepolymer solution through the channels and into the molds. The filled mold was crosslinked in a UV chamber for 20 s then the PDMS mold was carefully removed from the glass slide. The resulting PEGDA microwell array platform was immersed in phosphate buffered saline (PBS) overnight to equilibrate swelling of the hydrogel.

3.3.2. ECM protein coating

Collagen (Type I from bovine skin, fluorescein conjugate, Thermo Fisher Scientific) was prepared at a concentration of 0.1 mg/mL and loaded into sciFLEXARRAYER SX inkjet bioprinter (Scienion). A microarray of 400 pL droplets were dispensed, ensuring that the droplets aligned with the center of the microwells. After coating the inside of the microwells with fluorescein-conjugated collagen for ease of imaging, the microwell array was gently washed once with PBS

1X and incubated at 37°C overnight in a humidity chamber. Fluorescence imaging the following day confirmed that collagen remained adhered to the PEGDA microwells.

3.3.3. Diffusion properties

Hydrogel prepolymer solution was injected into 0.022" ID polytetrafluoroethylene (PTFE) tubing (McMaster-Carr) and crosslinked in a UV oven for 20 s. Water was then injected into the tubing up to the interface of the hydrogel and left to equilibrate for two days prior to testing. After two days, water was removed at the interface of the hydrogel in the tube and 0.1 mg/mL of 20 kDa fluorescein isothiocyanate-dextran (FITC-dextran, Sigma-Aldrich) was injected into the tube to the interface of the gel. Both ends of the tube were sealed with melted paraffin wax and the interface of the hydrogel was imaged over time.

3.4. Shallow flow cell fabrication and characterization

A 3D-printed master mold of shallow flow cells (SFCs) 40 μm in height was printed with the parameters described above and following the same post-processing protocol. PDMS base and curing agent were mixed at a 10:1 ratio. After degassing, the PDMS mixture was cast over the molds and cured in a 60°C oven overnight. Inlet and outlet holes were punched at both ends of the flow cell with a 1.5 mm punch. PDMS devices were sterilized by washing with 100% ethanol and rinsing with water, followed by UV sterilization.

3.4.1. ECM protein coating

A 10 ug/mL fibronectin solution in sterile, 0.22 μm filtered PBS 1X was prepared. 100 μL of fibronectin (bovine plasma, Sigma-Aldrich) was pipetted onto each sterilized SFC and incubated

at 37°C for 1 h. After the incubation period, the flow cells were washed gently with PBS and used immediately.

3.4.2. Capture slide functionalization

For the specific capture of EVs, a PolyAn 2D-Aldehyde slide (PolyAn) was functionalized with a cocktail of tetraspanin antibodies. Anti-CD63 (Biolegend), anti-CD9 (Biolegend), and anti-CD81 (Biolegend) were each diluted at 30 µg/mL in 0.22 µm filtered 1X PBS and mixed together for a total antibody solution concentration of 90 µg/mL. Cleaned SFCs were physically adhered to the PolyAn slide and 4 µL of antibody solution was injected into the flow cell. The antibodies were incubated at 70% humidity for 1 h, then blocked with 3% bovine serum albumin (BSA, Jackson ImmunoResarch) on a shaker at 450 rpm for 2 h, and dried before being used for experiments.

3.4.3. Particle tracing simulations

The single particle traces of EVs were calculated using a numerical computing application (MATLAB R2021a). The analysis was modelled on a two-dimensional chamber by assuming that a single point source at the center of the ceiling secretes an EV and the single EV diffuses to the bottom surface coated with antibodies which then immobilizes it. The diffusion was modelled as cumulative displacement composed of a series of orientations and step sizes, each with a time step of 0.1 s. At each step, the orientation was a unit vector randomly picked from a uniform distribution and the step size was a random variable of a Gaussian distribution $N(0,4D\tau)$, where D is the diffusion coefficient τ is time step. Binding kinetics were considered by introducing a binding probability that collectively represents binding kinetic parameters, including the dissociation constant and the surficial density of antibody. The binding probability determined whether the

single EV was immobilized upon contact with the surface, and in the case of failure, the EV continued the modelled diffusive displacement until immobilized. After iteration for multiple EVs, the final binding sites were plotted on a histogram for statistical analysis.

3.5. Cell culture and single cell loading

Green fluorescent protein (GFP)-transfected 293T human epithelial-like cells were cultured in Dulbecco's Modified Eagle Medium (DMEM, Gibco, Thermo Fisher Scientific) supplemented with 10% fetal bovine serum (FBS, Gibco, Thermo Fisher Scientific) and 1% penicillin-streptomycin (PS, Thermo Fisher Scientific). Cells were grown at 37°C in a humidified incubator (5% CO_2/95% air). Cells were harvested using TrypLE™ cell dissociation reagent (ThermoFisher) when 80% confluency was attained. The same volume of cell culture media was added to neutralize TrypLE™ before centrifuging down the cells at 200 rpm for 5 min. Cells were resuspended in fresh media supplemented with 5% exosome-depleted FBS (Fibco, Thermo Fisher Scientific) and 1% PS. The concentration of cell was measured by MOXI Z automated cell counter (Orflo) before dilution to the desired concentration. Cells were loaded by pipetting 5 µL of cell suspension solution on top of the desired platform and incubated at 37°C. After 2 h, nonadherent cells were gently washed away and fresh media was replenished for overnight incubation.

3.6. Cell viability assay

LIVE/DEAD™ viability/cytotoxicity kit (Thermo Fisher Scientific) was prepared according to the standard protocol. In this assay, live cells are stained with the esterase substrate calcein AM, while dead cells are stained with the membrane-impermeable DNA dye ethidium homodimer III. Prior to the assay, cells are seeded and cultured on the SFC for 24 h. Medium was removed from cells

and staining solution was added directly. Cells were incubated with the staining solution for 30 min at room temperature then imaged.

3.7. EV purification from cell culture

Cell media in flasks designated for EV purification was replaced DMEM supplemented with 5% exosome depleted FBS and 1% PS when cells were grown to 30-40% confluency. After an additional 2-3 days in culture, the cell media was removed from the flask and filtered with a 0.22 µm syringe filter. The filtered media was concentrated to 500 µL per 30 mL of cell media with ultracentrifugation filters (Amicon® Ultra-15-10k) centrifuged at 4000 rpm for 25 min. Size exclusion chromatography with qEV columns (Izon Science) was used to purify EVs. The columns were washed by flushing 6 mL of 1X PBS through the column, after which 200 µL of concentrated EV sample was added to the column and passed through using PBS as the buffer. 500 µL eluate fractions were collected for each column.

3.8. EV capture validation experiments

SFCs were washed in a water bath under sonication for 5 min and dried with nitrogen. The flow cells were placed on a functionalized EV capture glass slide and gently pressed down to ensure the PDMS was sealed to the glass. Epoxy glue was used along the edges to further ensure a tight seal to prevent leakage of fluid between the flow cells. 4 µL of purified EVs diluted in either 1X PBS or EV depleted DMEM media was injected into the inlet of each flow cell. 10 µL was further added to each the inlet and outlet to prevent evaporation during incubation. Purified EVs were incubated in each flow cell for 2 h at room temperature then washed twice with 1X PBS. A large

image of 6 x 6 fields of view (FOV) was taken of each flow cell at 60X magnification with fluorescence microscopy and the number of EVs in each FOV were counted.

3.9. Cell secretion time course experiment

SFCs with 293T-GFP cells seeded on the surface were left to grow and adhere for two days while incubated at 37°C with media changes daily. After two days, excess media was removed and the SFC was gently sealed onto a functionalized EV capture glass slide. Epoxy glue was used along the edges to ensure a tight seal and prevent leakage and evaporation. 3 μm Dynabeads® (ThermoFisher) diluted in EV-depleted DMEM media was added to the flow cell through the inlet and allowed to settle onto the surface of the glass for ease of focusing. Areas of interest were identified as FOVs containing only a single cell. The areas directly below the areas of interest on the surface of the capture slide were imaged by confocal microscopy at predefined time intervals. Time course cell experiments were performed in a live cell imaging chamber, controlling CO_2 and humidity.

3.10. Imaging and data treatment

All fluorescence images were taken with Nikon Ti2 confocal microscope using NIS-Elements Advanced Research software. Diffusion of FITC-dextran through PEGDA hydrogel was imaged over time and the spatial-temporal distribution of the diffusing dye was quantified with a custom MATLAB® script. For quantitative analyses of fluorescently labeled captured EVs, images were analyzed with another custom MATLAB® script. For each FOV, bright spots were identified based on a desired region of interest (ROI) size and by setting a threshold value where the spots could be confidently localized above the background. In validation experiments of bulk EVs, the

number of localized spots was averaged for all FOVs for each studied condition and the average number of spots per FOV and standard deviation were calculated. Error bars in EV counts represent the standard error of means (SEM) calculated by dividing the standard deviation by the square root of the sample size (number of FOVs). In time course experiments, EVs in a single FOV were counted cumulatively by localizing the positions of bright spots across all time points. Cell viability was counted using ImageJ software. Green and red channels were split to count live and dead cells separately. Images were converted into grey scale by thresholding and analyzed with the 'Analyze Particle' function. Cell viability was determined by dividing the number of live cells over the total number of cells and reported as a percentage.

4. Results

Two unique platforms were designed for the culture of single cells and direct imaging of their secreted EVs. The first consisted of microwells that physically isolate single cells from neighbouring cells, formed from a hydrogel material that allowed the inward diffusion of nutrients for long term culture yet prevented the outward diffusion of larger EVs. The second consisted of a shallow flow cell (SFC) that relied on spatial distribution to isolate single cells and a shallow gap between seeded cells and the EV capture surface to minimize lateral diffusion of secreted EVs. This section will summarize the design, fabrication, characterization, and use of both platforms.

4.1. HMA design, and fabrication

The Hydrogel Microwell Array (HMA) platform is designed to isolate and adhere individual cells to the ceiling of their microwells and image their secreted EVs with high temporal resolution as they are captured on the functionalized surface below (Figure 8A). This approach using hydrogels enables the diffusion of ions and small molecules in cell media outside the wells to promote long term cell culture within the wells and the ability to change cellular environments through fluid delivery. At the same time, the hydrogel can remain impermeable to larger EVs, up to several hundred nanometers in size, to concentrate them in their respective wells and prevent cross contamination of EVs from nearby cells. Cell secreted EVs diffuse across the microwell space, are captured and immobilized by a functionalized surface, and detected in over time by microscopy.

The microwells are embedded inside individual HMW PEGDA hydrogel pillars to enable the flow of media between each structure and ensuring the delivery of nutrients to each microwell (Figure 8A). Each microwell has a width and length of 80 μm to respect the lowest reliable xy-resolution

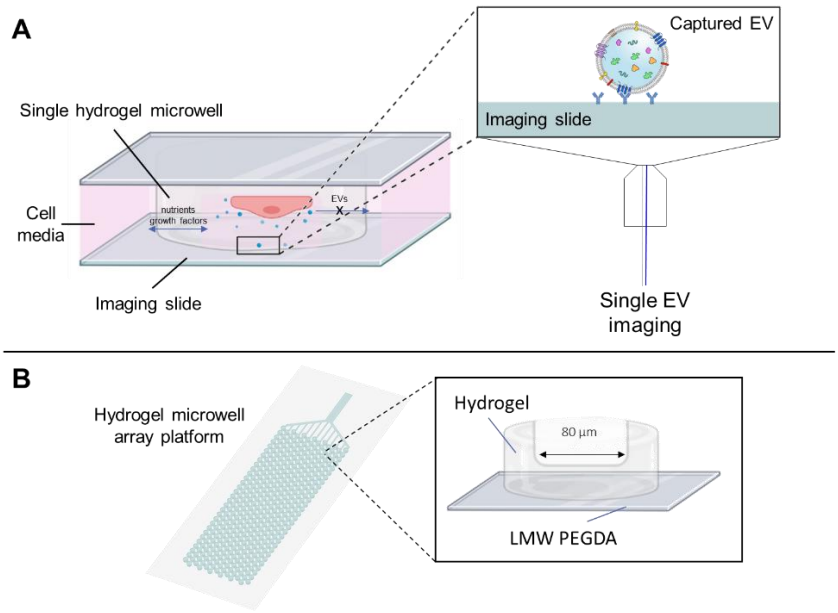

Figure 8. Schematics of the integrated single-cell HMA with EV capture on an imaging slide. **A.** EVs secreted by the single cell adhered to the ceiling of the hydrogel diffuse and bind to the antibody coated capture surface below. The use of hydrogel ensures the permeability of nutrients in cell media while preventing the permeability of smaller EVs. Live imaging detects the secreted EVs at different time points for high temporal resolution. **B.** The HMA platform which consists of 390 identical microwells with microwells in columns connected by a microchannel for prepolymer solution filling. Parts of figures created with BioRender.com.

achievable by the Tiger Apex 4K XHD PRO 3D printer and a depth of 40 µm to minimize the distance, and therefore diffusion time, between the cell sitting at the base of the microwell and the capture surface. Hydrogel pillars measured 320 µm in diameter and 80 µm in height and are spaced ~100 µm apart to allow the HMW PEGDA to swell when wet without touching adjacent pillars (Figure 12A). The array measures 3.5 mm x 9.5 mm and is arranged as 13 columns of 30 pillars. Each array accommodates a total of 390 identical microwells for isolating and concentrating EVs secreted from a single cell (Figure 8B). The volume of each microchamber is approximately 256 pL thereby concentrating the detected EVs in a small volume and ensuring high-sensitivity detection. All microwells in the same column were connected by a channel 120 µm in width and 20 µm in height to adapt a method called vacuum assisted UV micromolding (VAUM) for

hydrogel molding[175]. A schematic of the fabrication process of the HMA platform is depicted in Figure 9. A PDMS mold is cast from a 3D printed master mold using a 10:1 mixture of PDMS base and curing agent. An enclosed mold was assembled by placing the PDMS mold on a clean 3D printed LMW PEGDA surface to seal the cylinders and channels. LMW PEGDA contains poly(ethylene glycol) (PEG) monomers with which HMW PEGDA hydrogel can covalently crosslinked to without additional surface functionalizations. Additionally, as the surface is 3D printed, the inlet and outlet holes could be directly designed into the base. After enclosing the mold, photo-crosslinkable HMW PEGDA prepolymer solution was placed at the inlet and degassed to allow the solution to fully fill the cavities of the PDMS mold and be air-bubble free. After exposure to UV light for 20 s and demolding, a crosslinked HMW PEGDA HMA with the desired dimensions was created by replication from the PDMS mold.

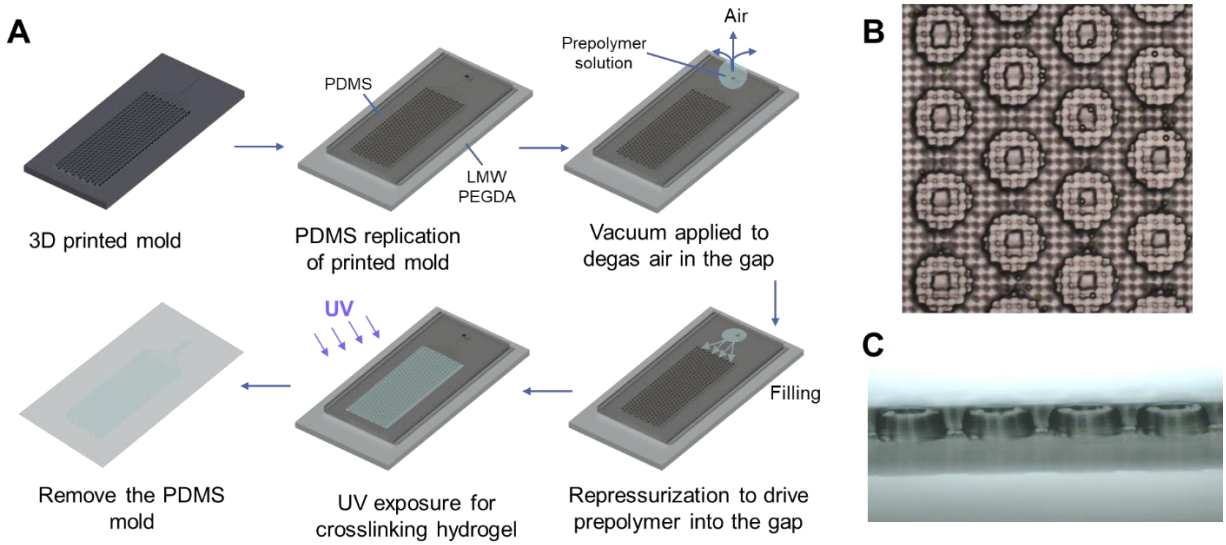

Figure 9. Molding and VAUM process for fabricating HMAs. **A.** Fabrication begins with a 3D printed mold from which a PDMS replication can be made. Then, an enclosed mold is assembled by placing the PDMS mold on a LMW PEGDA surface. The mold is degassed with a droplet of prepolymer solution at the inlet, then repressurized to fill the mold and UV crosslinked. **B.** Top view brightfield image of the hydrogel microwells. **C.** Side view differential interference contrast (DIC) image of individual hydrogel microwells.

4.2. Characterization of hydrogel microwells

Several criteria were developed to select an appropriate material to fabricate the HMA platform. First, the material must be biocompatible and support the growth of cells over several days for a time course experiment. Second, the material must be sufficiently robust to retain the molded features over time in cell culture conditions and resistant to cell degradation processes. Third, the material must be permeable to the diffusion of small molecules with hydrodynamic radii less than 10 nm, such as glucose, growth factors, vitamins, and minerals, yet be impermeable to the diffusion of EVs larger than 200 nm. Based on these criteria, photo-crosslinkable HMW PEGDA was chosen as the building material for this application, as it commonly used in biomedical applications, it exhibits excellent biocompatibility that has been widely studied[176–178] , and its mechanical modulus and porosity can be tuned by altering the PEGDA molecular weight or polymer density[179].

A range of PEGDA formulations was tested in order to identify one that can provide the balance between mechanical robustness and permeability required for our platform. Specifically, PEGDA with molecular weights of 700, 3400, and 6000 were evaluated as they are commonly used for cell-based assays[160,180–182]. It was observed that lower molecular weight PEGDA formulations (700) formed robust hydrogel microwells yet performed poorly towards the diffusion of small molecules. In higher molecular weight PEGDA formulations (3400 and 6000), FITC-dextran was observed to diffuse more yet remained sufficiently robust to retain the microwell features. Diffusion properties will be discussed in detail in the following section. Further increasing PEGDA molecular weight, however, results in increased system swelling which is not favourable for two reasons: first, small molecules have a greater distance to diffuse through as the hydrogel becomes thicker, and second, individual hydrogel pillars need to be spaced further apart to prevent them from touching and sticking, leaving more space for uncaptured cells to be lost during seeding. To

address the swelling that is observed in HMW PEGDA, PEGDA 6000 was supplemented with 10% hydroxypropyl acrylate (HPA). HPA contains acrylate groups that crosslinks with terminal acrylate groups on PEGDA. The greater extent of crosslinking creates a hydrogel network with greater integrity and less susceptible to swelling[183,184]. Finally, LAP was added as a photoinitiator for its reported biocompatibility, high water solubility, and high sensitivity to UV light[185]. Polymerization by UV light exposure allows for a fast and easy fabrication process. Combined with the described VAUM fabrication technique, only a small volume of prepolymer solution (4 uL for a 3.5 mm by 9 mm array) is needed to be injected inside the final mold.

Diffusion properties

As previously mentioned, the permeability of the hydrogel microwells is key to enabling long term cell culture within the platform. To evaluate the hydrogel for the diffusion of soluble molecules, the diffusion profile of FITC and FITC-Dextran was analyzed. Essential small molecules in cell culture media includes amino acids, vitamins, growth factors, and albumins, up to approximately 3.5 nm in size[186–188]. Specifically, 20kDa FITC-Dextran was chosen for its approximate hydrodynamic radius of 3.24 nm[189] and FITC alone was used as a control molecule. Figure 11 shows the movement of FITC and FITC-Dextran through the PEGDA hydrogel in a tube over 25 min. As expected, we observed that the larger 20kDa FITC-Dextran diffused slower through the hydrogel matrix compared to FITC controls that enter the polymer matrix more readily due to their smaller size. The corresponding spatial-temporal diffusion profiles were characterized as a function of distance from the hydrogel interface, where the fluorescent dye solutions were loaded (Figure 11A). Diffusion profiles here are shown across 800 μm, more than required for the thickness of hydrogels in the HMA when swelled, approximately 300 μm. It is also important to

note that the reported diffusion profiles were results of bulk hydrogels measuring approximately 550 µm in diameter. Hydrogel pillars in the HMA measure approximately 320 µm in diameter and only 80 µm in height. Although the resulting data is not completely representative of the HMA system, preliminary experiments on bulk systems presents a simplified approach that can deduce diffusion behavior of the hydrogel.

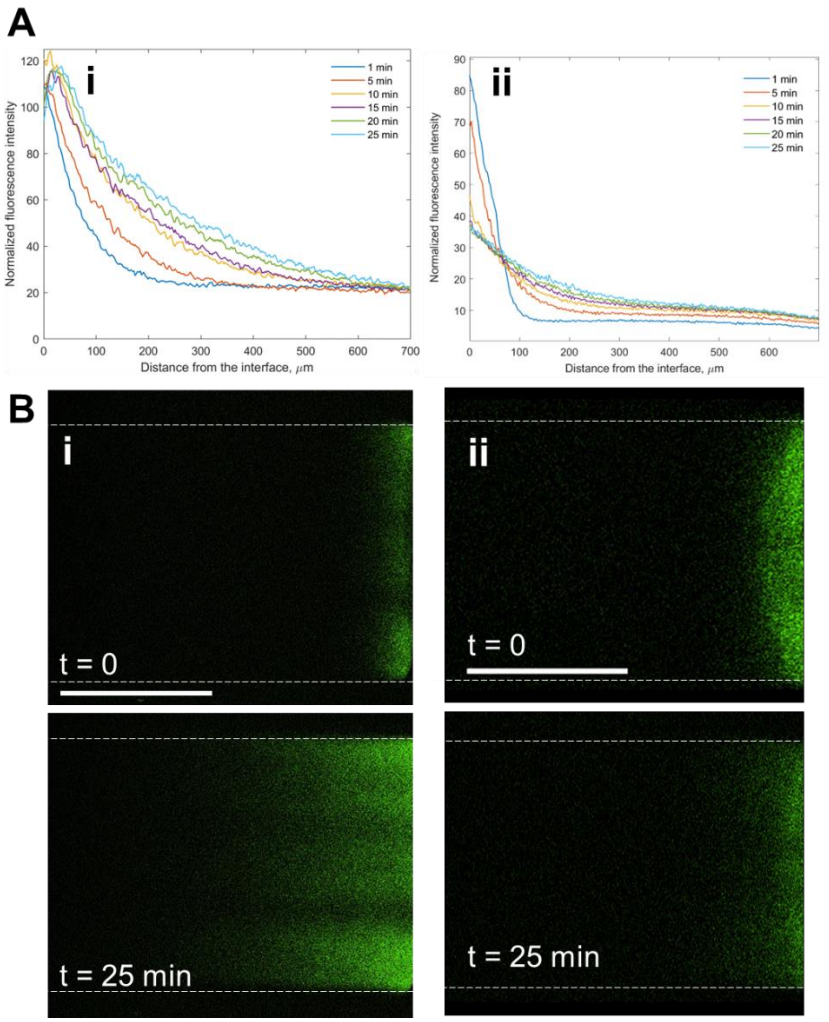

Figure 11. Characterization of the diffusion properties of PEGDA hydrogels. **A.** The diffusion profiles of **i.** FITC and **ii.** FITC-dextran as a function of distance from the interface of the hydrogel. (n=3) **B** Confocal images of **i.** FITC control and **ii.** FITC-Dextran (20kDa) diffusion in the hydrogels at t = 0 and t = 25 min Dashed lines indicate the edges of the PTFE tubing. Scale bars are 500 µm.

In addition, swelling of the hydrogel was observed inside the tube as the experiment progressed, despite allowing the gel to equilibrate in PBS for 72 h prior to experimentation. Most notably in the FITC-Dextran profile in Figure 11A, the decrease in normalized fluorescence intensity at a distance of 0 µm is a result of shift of the interface towards the left as the hydrogel swelled over time. This behavior can perhaps explain the only minor increase in fluorescence intensity over time and an inaccurately portrayed spatial-temporal diffusion profile, yet, confocal imaging of the FITC-Dextran sample (Figure 11B) does confirm that at a size of 20 kDa, FITC-Dextran was still able to partially diffuse through. However, the poor diffusivity of FITC-Dextran through the hydrogel matrix suggests that it may also be difficult for proteins such as albumins to travel through the hydrogel, while the permeability of the hydrogel towards FITC suggests that diffusion of small molecules such as vitamins and growth factors will not be hindered by the hydrogel matrix. In order to investigate a more permeable hydrogel, the formulation of the prepolymer should be modified with even higher molecular weight PEGDA or by reducing the concentration of PEGDA to create a network with greater mesh size.

Single cell loading in PEGDA HMA

PEGDA is natively resistant to protein adhesion and cell nonadhesive due to its hydrophilic and highly mobile poly(ethylene glycol) (PEG) backbone[181]. Yet, in order to prevent isolated cells from falling onto the imaging surface, cells in the HMA must adhere to the PEGDA ceiling of their individual microwells. It has been widely reported that PEGDA hydrogels can be modified with various cell adhesive ligands and proteins to support cell adhesion and proliferation[190–192]. Collagen is one of the main proteins found in the extracellular matrix (ECM) and is well known to significantly promote cell adhesion and proliferation[193]. In the HMA platform, it is specifically

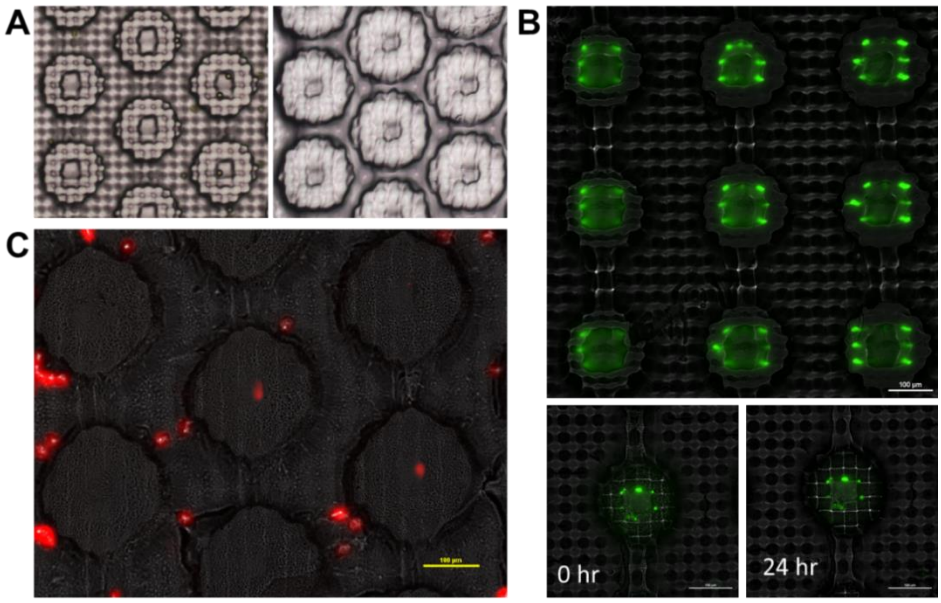

Figure 12. Swelling, patterning and cell seeding of hydrogel microwells. **A.** Hydrogels swell approximately 15% when wet (right) compared to their dry state (left), thus need to be spaced apart such that they do not touch when swelled. **B.** Precise patterning of the inside of individual microwells with fluorescein-conjugated collagen by inkjet spotting. Fluorescent collagen remains stable after 24 h of incubation. Scale bars are 100 µm. **C.** Cell seeding on the HMA. Two wells here contain a single cell seeded inside the microwells. Cells are labeled with DeepRed Cell Tracker Dye. Scale bar is 100 µm.

important to enable cell adhesion only inside the microwells and not in surrounding areas where they won't be isolated or on the surface of hydrogel pillars where they will be pressed against the capture glass. Piezoelectric inkjet printing is a systematic solution ideal for patterning biomolecules with precise control over both geometry and concentration. Collagen is prepared as the bioink and with the coordinates of the starting point aligned to the first microwell, it can be deposited as an array with high resolution according to the HMA design (Figure 12B). Collagen is coated by physical adsorption that occurs as a result of only weak Van de Waals and electrostatic interactions between the ECM protein and the hydrogel surface, therefore its stability over time was evaluated. As evidenced by the fluorescent signal that remains after a 24 h incubation and washing (Figure 12B), collagen appears to be successfully robustly coated inside the microwells. Cells are seeded by placing a droplet of cell suspension solution directly on top of the collagen

coated microwells and cells are given 10 min to settle into the microwells (Figure 12C). Single cell loading efficiency, calculated as the number of microwells containing a single cell after seeding over the total number of microwells, was approximately 20% with 50% of microwells containing zero cells. Given the HMA accommodates 390 microwells, there can ideally be up to roughly 80 isolated cells per platform.

Transition to the Shallow Flow Cell platform

The two main innovations behind the HMA platform were the microwell design to physically isolate cells and confine their secreted EVs, and the use of a hydrogel material to control diffusion and delivery of nutrients to cells. While the HMA platform successfully achieved cell compartmentalization, challenges were faced when moving forward to cell seeding and long-term culturing particularly concerning a lack of diffusion. These roadblocks are examined in further detail in Section 5. Rather than restarting at square one and reoptimizing the formulation and fabrication process to address these issues, it was decided that additional work to perfect the HMA platform outweighed the merits. Instead, a second platform fabricated from PDMS and based on a single shallow chamber that would isolate cells spatially was proposed. Details of the platform approach are outlined in Section 4.3. Use of the new Shallow Flow Cell (SFC) platform ultimately eliminates the use of hydrogel and individual confinement, thereby eliminating both the difficulties that came with seeding individual microwells and diffusion across the hydrogel. As a result of the shift in direction, all subsequent work presented in this thesis will be performed with the SFC platform.

4.3.SFC design and fabrication

The SFC is a simplified platform designed to have a large surface area to distribute cells at a low density such that single cells are spatially isolated from one another. Similar to the HMA platform, cells will be adhered to the ceiling of the flow cell and secreted EVs will be captured and detected on a functionalized surface directly below under stop-flow conditions (Figure 10). The chamber has a height of 40 µm, conducive to EV binding following diffusion onto the capture slide with characteristic diffusion time of tens of seconds, and minimal lateral diffusion of EVs. Adequate distribution of single cells across the entire flow cell will prevent cross contamination of EVs secreted by neighbouring cells as EVs will be more likely to be captured and immobilized by the capture surface than diffusing laterally between fields of view (FOV). By setting the FOV directly under the spatially isolated cell, EVs can be detected with high temporal resolution and associated back to their cell of origin. To maintain cell viability, media can be flushed through the flow cell between imaging timepoints. EVs secreted during media exchange (few seconds) will be lost, hence, media exchange frequency can be optimized towards minimal EV loss.

The SFC is cast from a 3D printed master mold using a mixture of 10:1 PDMS base and curing agent. The ellipse flow cell measures 9 mm in length and 4 mm in width, with a height of 40 µm. As the flow cell is shallow and risks collapsing when bonded to the functionalized glass surface, an array of 140 µm diameter pillars was embedded throughout.

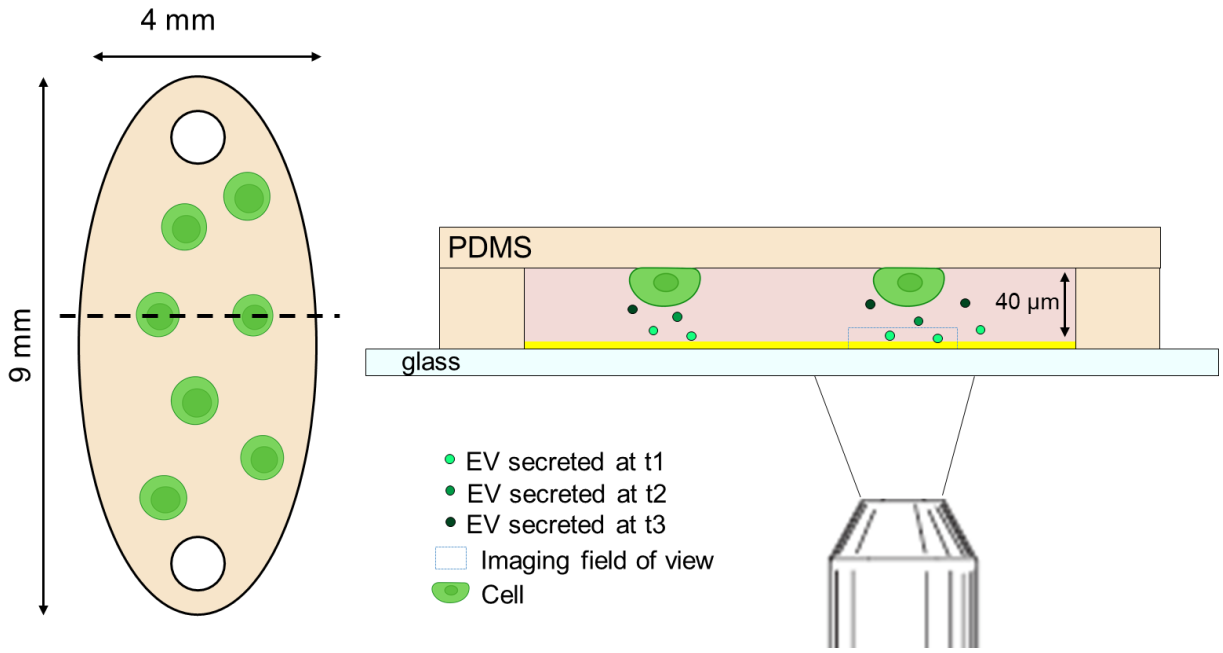

Figure 10. Schematic of the SFC platform. Endogenously labeled single cells are spatially isolated and adhered to the ceiling of the flow cell. Secreted EVs are imaged directly below at high temporal resolution. Enlarged image on the right shows a cross section of the platform indicated by the dashed line.

4.4. Characterization of the SFC

Cell seeding on PDMS

PDMS is widely used in microfluidic devices for bioassays for its biocompatibility, gas permeability, and optical transparency[194]. The main drawback of PDMS devices in cell biology is its intrinsic high surface hydrophobicity that strongly influences surface wettability and cellular attachment. To overcome this limitation, several surface modification methods have been developed to increase the hydrophilicity of PDMS for facilitating cellular adhesion and proliferation. In physiological conditions, ECM proteins, such as collagen, gelatin, and fibronectin, possess various cell adhesion moieties to promote cell attachment. Reportedly, fibronectin has the highest rate of protein adsorption onto PDMS[195–197] and was therefore selected to coat the SFC. Different fibronectin coating protocols were tested, mainly to evaluate the effect of pre-activating

the PDMS surface with oxygen plasma and incubating fibronectin on the surface at various temperatures. Cell spreading differences of 293T epithelial cells are clearly shown in Figure 13A and surprisingly, greater cell spreading was observed on PDMS surfaces only coated with fibronectin compared to surfaces pre-activated plasma combined with fibronectin coating. Visually, the optimal cell spreading was determined to be on the fibronectin surface not preactivated with plasma and where the fibronectin was incubated at 37°C prior to cell seeding. Further culture of cells grown on the optimized fibronectin coated PDMS surface is shown in Figure 13B where cells showed healthy proliferation and growth to confluency on the surface after four days.

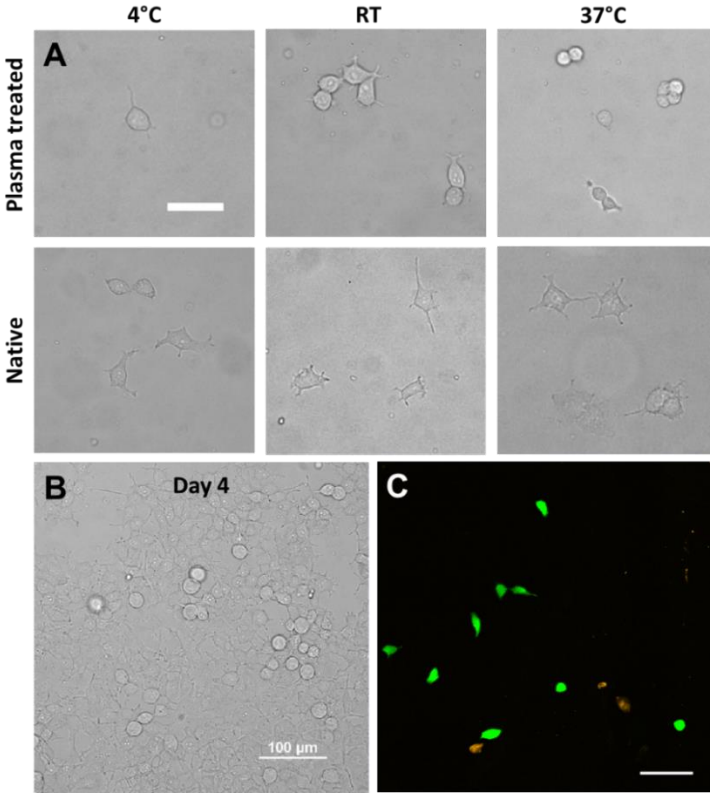

Figure 13. Cell seeding on the PDMS SFC platform. **A.** The capacity of the fibronectin-coated surface prepared by different coating conditions to promote cell adhesion was inspected by verifying cell spreading and adhesion. Scale bar is 50 µm **B.** Long term cell culture of 293T cells on PDMS surface treated with fibonectin incubated at 37°C after 4 days showing high cell growth and healthy cell spreading. **C.** Cell viability after 24 h of culture. Fluorescent images of LIVE/DEAD stained images of cells grown on PDMS where live cells appear green (488 nm) and dead cells are orange (555 nm). Scale bar is 100 µm

Short- and long-term cell viability

Cell viability of 293T cells on the SFCs was assessed using a LIVE/DEAD™ assay on cells cultured on the fibronectin coated flow cell over 24 h. Cell counting was done using ImageJ, giving a total cell count number of cells in the 460 nm green channel (live) and cells in the 555 nm orange channel (dead). Result of the assay indicated 88% cell viability across cells seeded on three separate flow cells (n=105). Confocal images of live cell morphology further confirm that 293T cells are able to spread and grow on the fibronectin coated SFCs (Figure 13C).

Particle tracing simulations

Computational modelling of particle tracing inside the SFC showed that with the given parameters, almost all particles secreted from the ceiling of the flow cell are captured on the surface below within one experimental FOV. The flow cell was simulated with a height of 25 μm, modeled from confocal images measuring the distance between a cell spread and adhered to the ceiling to the capture surface below (Figure 14A). In the model shown in Figure 14B, *N* secreted particles are initially at one point on the ceiling of the simulation box. They diffuse between the ceiling and the bottom surface, on which a static array of binding sites is located. Upon contact with the surface, the binding probability determined whether the particles would bind irreversibly to the bottom surface, and if not bound, the particle continued the modelled diffusive displacement until immobilized. The simulation assumed a no flow condition within the chamber, allowing the particle motion to be entirely dictated by Brownian motion and diffusion. The binding probability considers binding kinetics and collectively represents parameters including dissociation constant and the surficial antibody density. After iteration for multiple particles, the final binding sites

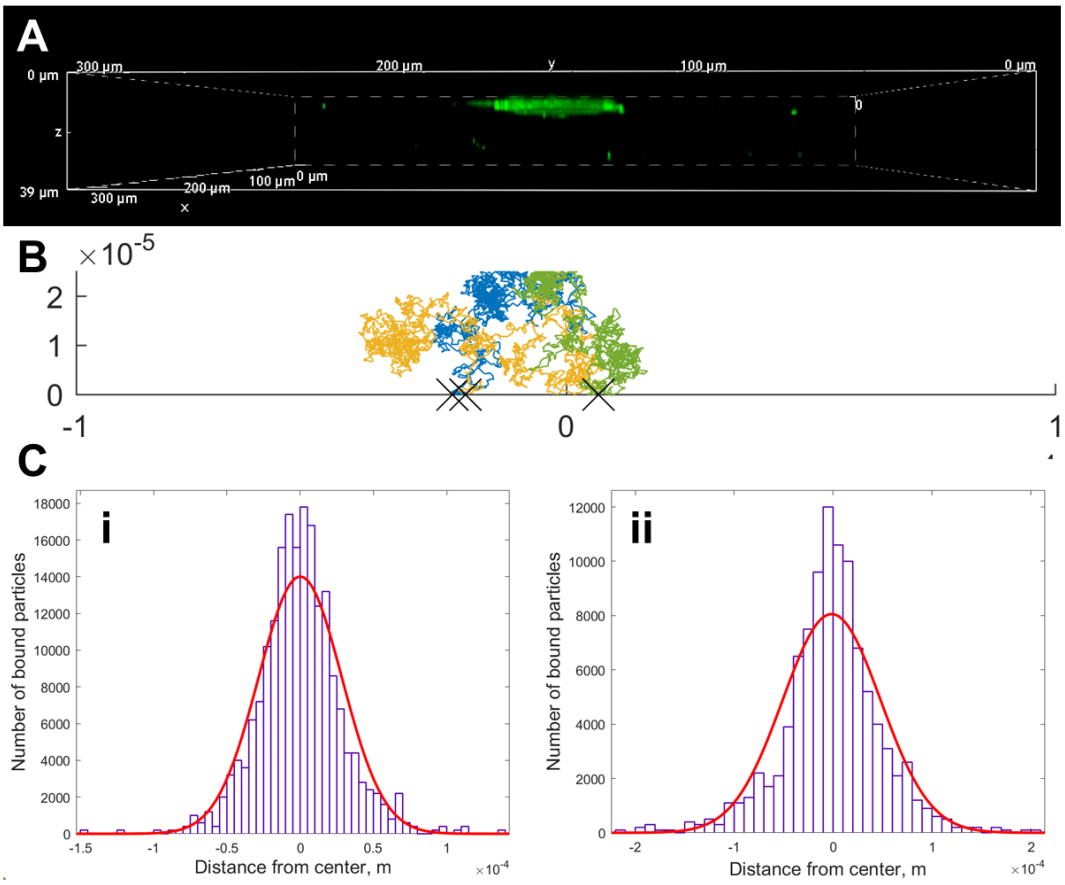

D

Binding probability	Length of 95% binding area, µm
0.1	113.90
0.01	195.10
0.005	261.52

Figure 14. Simulation of particle tracing in the SFC platform. **A.** Z-stack volume projection confocal imaging of the inside the 40 µm deep flow cell. A single 293T-GFP cell spread and adhered to the ceiling of the SFC. **B.** Particle tracing simulation showing traces of three particles (coloured) secreted from a point on the ceiling, their diffusion across the chamber, and immobilization on the bottom surface (marked by an X) when the binding probability is 0.1. On the x-axis, 0 indicates the position directly below the point of secretion **C.** Histograms of the distribution of particle final binding sites, fitted with a normal distribution (red) when the binding probability is **(i)** 0.1 and **(ii)** 0.01. **D.** Summary of the area where 95% of secreted particles in the simulation bound to the surface with decreasing binding probabilities. As the simulation is run in 2D, length indicates the range in the x-axis where particles were bound.

were plotted on a histogram for statistical analysis (Figure 14C). As the binding probability cannot be empirically determined, arbitrary binding probabilities based on calculations with classical

diffusion mass transport were inputted and compared. Details of these calculations are outside the scope of this thesis but will be further discussed in a future manuscript by Kim et al. The chosen binding probabilities are far below reported values in from computation models to investigate the lower threshold of the system[198]. The histograms demonstrating the possible outcomes of EV binding sites were fitted with a normal distribution and the 95% confidence interval was determined. This range indicates where 95% of secreted particles will be bound to and is summarized in Figure 14D. As one imaging FOV at 60X magnification is approximately 250 μm by 250 μm, we expect 95% of secreted particles to bind within one FOV even with a binding probability as low as 0.005. Our particle tracing simulation supports our confidence that the almost all cell secreted EVs will be captured on the imaging surface below as only 5% of secreted EVs is expected to be lost outside of the FOV due to lateral diffusion.

4.5. Validation of EV detection

Optimization of EV immobilization

The principle of antibody-based EV capture and detection within the SFC platform was initially assessed at a bulk level with purified EVs. First, the EV immobilization strategy would affect the result of EV analyses, so an optimized immobilization surface is demonstrated here. If EVs are immobilized using a single targeted antibody, captured EVs will only reflect EVs positive for that protein marker and the results will not be reflective of the entire population of EVs. Therefore, to increase both the shear number and diversity of captured EVs, the advantage of surface immobilization with a combination of antibodies was explored. Endogenously GFP-labeled EVs harvested from 293T cell culture media were diluted in media and immobilized on one surface coated with only CD63 antibodies and another with a cocktail of CD9, CD63, and CD8 tetraspanin

antibodies. Both EV-immobilized surfaces showed clear single-EV images. When the number of each EV signal was quantified and compared, with the same concentration of EVs introduced to each surface, the tetraspanins cocktail capture sample showed distinctly higher counts of EV signals compared to the single anti-CD63 capture sample (Figure 15A). This demonstrates that a cocktail capture strategy provides both a greater amount of capture as well as more diverse results in terms of captured EV population.

To further verify the capture antibody functionalization, the cocktail capture surface was compared to one coated with only 3% BSA to passivate the surface. Additionally, the complexity of cell culture media and the effects of its added supplements on EV surface capture was investigated. EVs harvested from the same population of endogenously labeled 293T-GFP cells were diluted into either PBS or EV-depleted cell culture media, flushed into their respective chambers, incubated for 2 h, and washed. The resulting fluorescent regions and the immobilized EVs were then visually inspected and enumerated. At least 25 FOVs were imaged and counted for each condition and averaged. First, images of control surfaces, where just PBS or media was flushed in, revealed little to no fluorescence signals, indicating that EVs were not present on the surface (Figure 15B). In contrast, confocal images of EV-immobilized surfaces showed distinct EV-like signals (Figure 15C). Regions blocked by BSA showed less than 140 EVs per FOV, while the immobilized EVs captured by the functionalized surface showed over 400 EVs per FOV. These results demonstrate substantial blocking of nonspecific EV binding from the BSA-passivated areas and the successful immobilization of EVs at the functionalized areas. Furthermore, the capture of EVs in media is similar to the capture of EVs in PBS, indicating that additional proteins and

molecules in cell culture media that are essential for long term cell culture do not hinder the binding of EVs to the capture surface.

Evaluating the capture of low EV concentrations

Next, the capacity of the platform to quantify low counts of EVs expected from a single cell was assessed. A series of control experiments were performed to estimate the ability of the platform to capture and detect known concentrations of EVs. EVs harvested from cell culture media were quantified by NTA to determine the concentration of particles in solution. EVs were then diluted 10-fold and 50-fold in PBS before being flushed into flow cells so the number of captured EVs from different known dilutions of EVs can be compared to the expected count. The expected number of EVs was calculated from the known volume of EVs, total area of the capture surface below each flow cell, and the area of a single imaging FOV. Additionally, it was assumed that the distribution of EVs throughout the flow cell was homogeneous. At the three concentrations of purified EVs investigated, the analysis of ~10 confocal images per dilution showed that after a 2 h incubation followed by washing, the counted number of EVs is similar to those obtained from calculations (Figure 15D). Few EVs may be lost as the flow cells are washed post incubation, yet the majority of EVs appear to remain on the imaging surface. With these observations, we conclude that the functionalized surface successfully immobilizes most of the EVs in the flow cell.

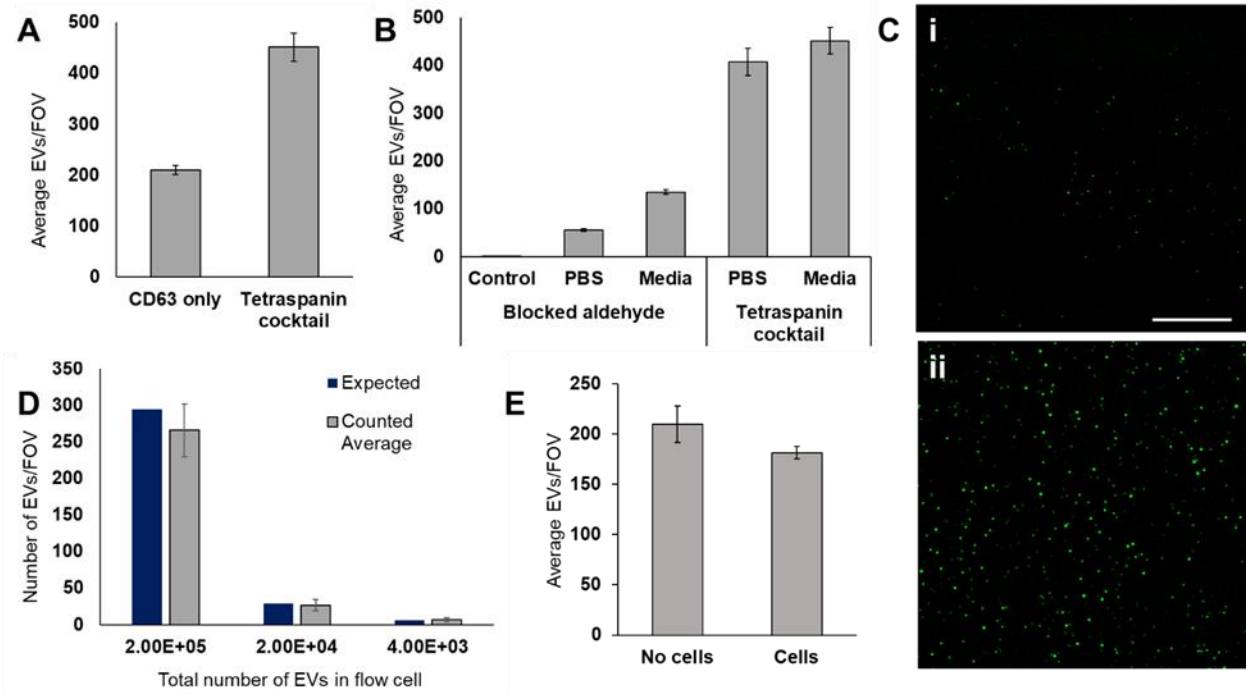

Figure 15. Validation of SFC platform and capture surface for EV immobilization. **A.** Comparison of EVs captured per FOV on a surface coated with only CD63 antibodies and one coated with a cocktail of tetraspanin antibodies. **B.** Comparison of EVs captured per FOV on a blocked aldehyde surface and a surface coated with a cocktail of tetraspanin antibodies when EVs are diluted in PBS and media. Capture by the tetraspanin cocktail surface was much greater. Control indicates no EVs were injected into the flow cell. **C.** Confocal images of EVs diluted in media injected into the flow cell and **i.** non-specifically adhered to a blocked aldehyde surface as a negative control and **ii.** captured by a surface coated with a cocktail of tetraspanins antibodies **D.** Comparison of EV capture count at different known dilutions of purified EVs to the expected number of EVs per FOV. Total number of EVs in flow cell was determined based on the known volume and concentration of EVs. Expected number of EVs/FOV was calculated by dividing the total number of EVs by the total surface area below the flow cell and the area of a single FOV. Counts of EVs from three flow cells were averaged. Differences between the expected number and the counted average are low and indicates that nearly all EVs are captured. **E.** Comparison of the capture of purified EVs injected into the flow cell on a tetraspanin cocktail antibody coated surface in the presence and absence of cells and fibronectin are coated on the ceiling. No significant differences between the two conditions indicates that EVs minimally lost to the coated ceiling surface. All error bars indicate standard errors of means (SEM).

Effects of fibronectin coating on EV capture

To demonstrate that EVs will not be lost due to interactions with the fibronectin coating of the SFC platform, purified endogenously GFP-labeled EVs were flushed into flow cells containing cells adhered to fibronectin on the ceiling. The fibronectin coating protocol was performed as

previously described and cells were seeded at a low density after 1 h of fibronectin coating. Cells were incubated at 37°C overnight to allow for adhesion and spreading before sealing the flow cell closed with an anti-CD63 functionalized glass capture surface. The same concentration and volume of purified GFP-EVs were flushed into a bare flow cell without any surface treatments and sealed with the same anti-CD63 functionalized glass capture surface. After a 2 h incubation followed by washing, the average number of EVs detected per FOV in the cell coated chamber compared to a bare chamber decreased by only 13% or an approximately 13% loss of EV capture due to fibronectin (Figure 15E). As demonstrated by the proportional of positive signal still achieved in the cell seeded chamber, the majority of EVs were still able to be captured on the functionalized glass surface. This indicates that EV capture on the imaging surface is not substantially affected by the presence of fibronectin.

4.6. ‘Real-time’ capture and detection of EVs

To assess the functionality of our time-resolved analysis platform, a low concentration of purified EVs was introduced into the SFCs to mimic EVs secreted from a single cell. Dynabead® magnetic beads were used to facilitate image focusing on the surface of the capture platform and a 1 µm Z-stack was taken at each FOV of interest. FOVs were imaged every 2 min over an 80 min period to capture immobilization of EVs on the surface at high temporal resolution. Fluorescence signals started appearing soon after injecting the EVs (Figure 16). Few signals were seen to be almost instantly captured by antibodies on the capture surface before latter EVs diffused across the chamber to reach the surface. At each time point, the captured EVs were localized and counted in each FOV of interest. Some EVs did not change in localization over time, suggesting robust immobilization, whereas many signals disappeared in subsequent frames.

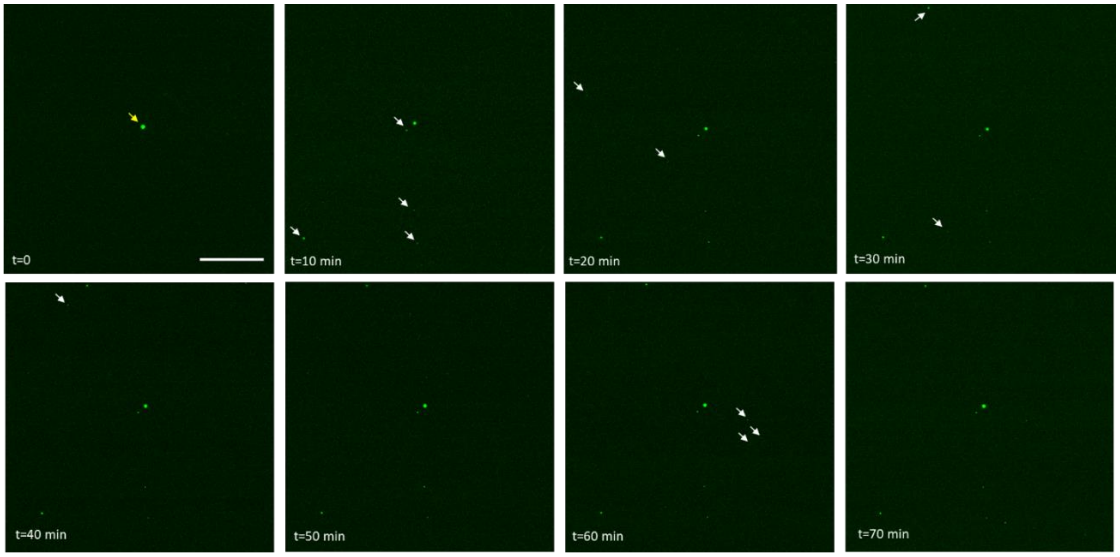

Figure 16. Confocal images of a single FOV at the capture surface showing EV immobilization over time. A magnetic bead (annotated by the yellow arrow) at the center is used for focusing and the annotated white arrows indicate fluorescent EV signals as they appear. Signals that remain over time are not annotated in subsequent images. Scale bar is 50 μm.

Time course capture of EVs

Results from six FOVs were pooled together to analyze the times of EV capture, and the binding of EVs to the surface. In Figure 17A, time of capture describes at which point during the 80 min experiment an identified EV was captured on the surface. The majority of EVs were found to be captured within the first 10 min of the experiment, and we observe a sharp decrease after 30 min. The system then appeared to reach a steady state after approximately 40 min. These results provide information to support the assumption that there is little to no flow within the system, therefore, EV capture is reliant on diffusion. Initially, the EVs close to the surface of the glass will diffuse towards the surface and be captured. The rate of EV capture then decreases as the EVs near the surface have been depleted, and remaining EVs must diffuse across the platform. A constant rate of capture was seen after 40 min. Additionally, as the experiment progresses, EVs may also diffuse towards the ceiling of the PDMS and be lost to adhesion, resulting in a lower count of EV capture over time.

EV surface affinity

Another aspect of EV capture that was analyzed was the affinity of EVs to the capture surface. Robust binding affinity is essential as monitoring real-time rate of secretion relies on the cumulative collection of EVs over the analysis period. In Figure 17B, residence time describes the duration of time an EV was localized in the same FOV, where higher residence time indicates a strong immobilization of the EV to the capture surface. Almost 70% of captured EVs had a residence time of less than 10 min, suggesting high dissociation of captured EVs. EVs may not be tightly bound to the antibodies on the glass surface due to an antibody's high dissociation constant (k_{off}). k_{off} is a measure of how quickly an antibody dissociates from its target. A high k_{off} results in quick dissociation time so the EV is released and able to diffuse away from the surface. Because a cocktail of different antibodies is used the k_{off} of each antibody differs and it is difficult to characterize each one without individual investigations. Residence time is also, however, a biased measurement due to the duration of experiment. For example, as analysis only ran for 80 min, EV captured at 40 min could only record a maximum residence time of 40 min.

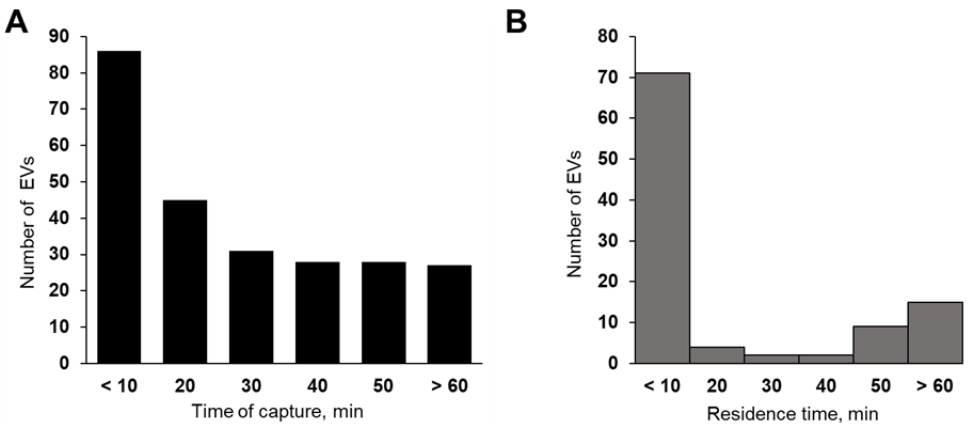

Figure 17. Quantified EV signals throughout a time course analysis. **A.** Time, based on imaging frame, when identified EVs are captured by a cocktail of tetraspanins antibodies (n=6). Almost 70% of EVs are captured within the first 10 min of the experiments and a steady state is reached after approximately 40 min. **B.** Distribution of residence times of single EVs imaged on the capture surface (n=6). Most EVs bind and detach within 10 min, while a significant fraction stayed bound for over 60 min.

4.7. Proof-of-concept time course detection of cell-secreted EVs

As a proof-of-concept experiment, the performance of the platform for time-resolved EV secretion analysis by a single cell was assessed. 293T cells were cultured on the SFC platform for 48 h before the chamber was sealed to a tetraspanin cocktail of antibodies coated on glass slide for EV capture. A single cell with healthy morphology was identified and its position was registered (Figure 18A). The Z-position was then moved below the single cell to focus on the glass surface, using Dynabead® magnetic beads for ease in focusing. The captured EVs on the surface were imaged every 15 min over 2 h to quantify the rate and abundance of EV secretion by a single cell over time (Figure 18B). Although imaging can be achieved in almost real-time at intervals on the scale of seconds, analysis of cell secretions here should be described as quasi-real-time as we must take into consideration the diffusion lag between the time of secretion and time of capture on the surface, and our time between imaging on the scale of minutes. Similar to what was observed in the validation experiments with purified EVs, robust affinity of EVs to the capture surface was found to be low. Figure 18B shows images of the first several time points of the secretion experiment. Most localized EVs were not observed in subsequent imaging frames, suggesting that they were not strongly immobilized. Still, the captured EVs in each frame were quantified and a summary of EV secretion over time is shown in Figure 18C. Heterogeneity in the number of secreted EVs at each time point was observed, with the greatest number of EV capture after 60-75 min. Based on the data, we can interpret a single cell secretion rate of approximately 10 EVs/h, however, heterogeneity in EV capture suggests that secretion is not occurring at a regular rate. The reported rate is specific for a 293T cell in steady state conditions, and we expect rates to differ between cell types and cellular environments. As very few EVs were observed over the 2 h, and there is uncertainty whether EVs captured in later frames are newly secreted or the recapture of

dissociated EVs, further statistics on EV secretion rate were not determine at this time. Nevertheless, we demonstrate that, as a platform technology, EVs secreted directly from single cells can be imaged with high temporal resolution.

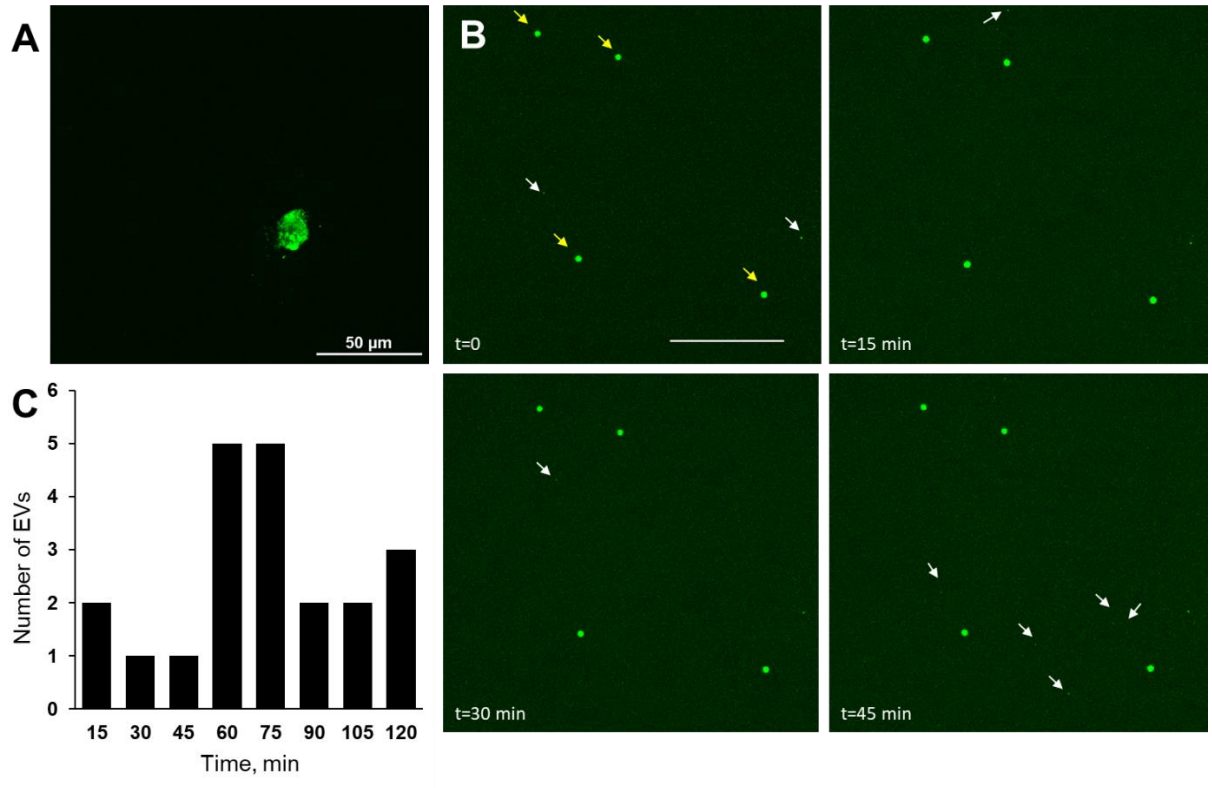

Figure 18. Time course detection of secreted EVs from a single cell imaged at 15 min intervals. **A.** A single 293T-GFP cell adhered to the ceiling of the SFC platform. **B.** The antibody functionalized surface directly below the area in panel A. x- and y- coordinates of the FOV are identical to those in panel A, while the focus is approximately -25 µm in the z-axis. Confocal images were taken at different time points to observe secreted EVs over time. A subset of images is shown with larger magnetic beads (annotated with yellow arrows in the first frame) for focusing and captured EVs annotated by white arrows as they appear over time. Scale bar is 50 µm. **C.** Time, based on imaging frame, when cell secreted EVs were captured on the imaging slide. The highest number of EV capture was seen after 60-75 min of incubation, however, there is uncertainty whether the captured EVs are freshly secreted or rebinding of existing EVs.

5. Discussion

Here, two platforms were developed for time course imaging of single cell EV secretions at the single particle level. In these two designs, single cells and their secreted EVs can be isolated either by compartmentalization or spatially. Both platforms presented here leverage endogenously labeled cells and EVs to enable direct imaging of cells and secretions without the need for additional labeling steps. Although this bypasses the lag between secretion and detection caused by exogenous labeling and washing steps, we acknowledge there is still a diffusion lag within our platforms limiting true 'real-time' secretion analysis. However, because we can visualize single EVs as they are being captured on a surface over time, we can use the described platforms to conduct time course experiments to deduce EV capture rates. In this manner, the dynamics of EV immobilization on a capture surface have been investigated using purified endogenously labeled EVs to validate our platforms' imaging capabilities.

Novelties and advantages of the HMA platform

The first platform presented was the HMA. The two main innovations behind the HMA platform were the microwell design to physically isolate cells and confine their secreted EVs, and the use of a hydrogel material to control diffusion and delivery of nutrients to cells. Cell compartmentalization is a traditional method for isolating single cells, however, most other platforms are unable to resolve single cell secretions to the single particle level, as the HMA platform is designed to. Such microwell platforms and microfluidic devices also rely on photolithography as a fabrication method, requiring a cleanroom and complex equipment[158,160], whereas the preparation of the HMA platform demonstrated here does not require any microfabrication techniques. A major advantage of our fabrication process is that it is much more

simplified, relying only on 3D printing, soft lithography, and the VAUM process which uses readily available instruments. Moreover, experiments with the HMA platform can be run and imaged directly on a conventional confocal microscope.

Challenges faced with HMA platform

As the HMA platform was being developed and optimized, a number of unexpected hurdles arose that hindered its application for biological studies. First, imaging preparation was tedious and experimental throughput was found to be low due to low seeding efficiency. For each 6400 μm^2 of microwell area where the cell could be loaded, there is 89 600 μm^2 of surrounding area where the cell can land and become unusable for secretion experiments. With only ~20% of microwells containing a single cell after loading, the microwells of interest must be identified for each experiment manually before programming the imaging software to sequentially move between the desired FOVs for time course imaging. In a single platform where all conditions can be kept consistent, including fibronectin coating density, antibody coating density, and environmental conditions, having multiple cells for analysis is important to achieve multiple repeats to confirm findings and identify outliers. Without a robust system for conducting multiple repeated experiments, it is difficult to confidently compare different environmental conditions in cell studies.

The biggest roadblock when optimizing the HMA platform were the challenges faced with the diffusion properties of the hydrogel. The poor diffusivity of 20 kDa FITC-Dextran shown in section 4.2 raises concerns regarding the ability of cell media components to diffuse through the hydrogel and reach the single cell in culture. As a time course secretion profiling experiment relies

on the healthy long-term culture of cells, small molecule diffusion through the hydrogel was an essential element of the HMA platform. Rather than restarting at square one and reoptimizing the hydrogel formulation to address the issue, as well as given the aforementioned challenges, it was decided that additional work to perfect the HMA platform outweighed the merits. Instead, a second platform fabricated from PDMS and based on an open concept flow cell that would isolate cells spatially was proposed. Details of the platform approach are outlined in section 4.1. Use of the new PDMS platform ultimately eliminates the use of hydrogel and individual confinement, thereby also eliminating the challenges that came with seeding individual microwells.

Advantages and challenges of SFC platform

The second platform presented in this work is the SFC. Platform fabrication was further simplified as the flow cell requires only one-step soft lithography with PDMS from a 3D printed mold. While the design and fabrication of the SFC was much simplified, operation of the platform was not without challenges. First, the intrinsic high surface hydrophobicity of PDMS causes poor cell adhesion and therefore must be reduced to facilitate long-term cell studies. One method to achieve a more hydrophilic cell adhesive surface is with an ECM protein coating. We show optimized fibronectin protocols for the PDMS SFC platforms that enabled healthy cell adhesion and spreading on the ceiling of the flow cells as verified by cell viability assays and fluorescence microscopy. Although fibronectin was essential for cell adhesion to PDMS, one concern of the ECM protein coating was the loss of captured secretions due to EV adhesion to the ECM surface. Further experiments revealed lower EV counts in flow cells coated with fibronectin, suggesting that certain EVs bind to the coated ceiling, as supported by reports of subpopulations of EVs expressing higher levels of fibronectin on their surface[199–201]. Although some EVs may be

unaccounted for due to adhesion to the ceiling, a rate of secretion experiment comparing secretions by single cells induced by external stimulations remains unaffected since it can be assumed that individual cells lose the same number of EVs. Furthermore, experiments within the SFC platform rely on no-flow conditions to minimize lateral diffusion of secreted EVs and their capture in the FOV directly below the secreting cell. Attempts to control a static environment within the chamber were made by ensuring large liquid droplets at the inlets and outlets to prevent evaporation of the liquid within the chambers. To confirm zero flow conditions however, additional efforts will need to be made to quantify flow in the chamber with beads and particle tracing experiments.

Considerations to spatial resolution in microscopy imaging

Spatial resolution plays an important role in confirming our ability to resolve EVs at the single particle level and to differentiate closely binding EVs from EV clusters. With our fluorescence confocal microscope, 100 nm liposomes have been experimentally imaged successfully. 100 nm is similar to the expected size of secreted EVs, allowing us to interpret the fluorescent dot signals as single EVs with confidence. Additionally, from early validation experiments using fluorescent beads prior to EV experiments, we were able to image 50 nm beads both in solution and when settled onto a surface. Individual beads were optically resolvable from one another even when they landed approximately 100 nm apart (data not shown here). As a result, unless EVs are binding within approximately 100 nm of one another, we can confidently assess the signal as a single EV. Given the low abundance of EVs in our experiments, only a few EVs released in the span of 10 minutes in a chamber containing ~0.9 μL of media, it is unlikely that EVs will bind within 100 nm of one another or interact and bind with one another in solution to form a cluster. This is seen in our experiment detecting single EVs secreted from a single cell. EVs imaged on the surface were

typically separated by 50 µm, with the closest two EVs being approximately 10 µm apart (Figure 18B). While it is possible that EVs are directly released as clusters, it has not been found to be an issue in most literature reported single EV studies. In the case that larger clusters are secreted or formed, they can be investigated by looking at the size and shape of the fluorescent signal and eliminated during data processing if necessary.

Shortcomings of time course imaging experiments

As we are interested in quantifying the secretions that diffuse downward and are captured and imaged on the glass surface, efforts were made to optimize the binding of EVs. EV capture using a cocktail of tetraspanin antibodies showed high levels of EV immobilization compared to capture with only CD63 antibodies. Using a mixture of antibodies, a wider population of EVs could be analyzed, rather than only EVs bearing specific epitopes. However, in later time course experiments, a high degree of EVs signal loss was observed. This may be a result of the unbinding of EVs from the capture surface, yet it is difficult to attribute a high dissociation constant to one antibody species in particular due to the use of multiple antibodies. Additional control experiments where surfaces are coated with only anti-CD9 and only anti-CD81 will be beneficial to determine which antibody has larger binding constants and promote stronger EV affinity. It is also important to consider photobleaching as a reason for EV signal loss. Although possible, we don't expect a large degree of photobleaching with the presence of multiple fluorophores and low imaging power, and loss of signal is believed to be more consistent with EV unbinding. Lastly, loss of signal could also be a result of inaccuracies in imaging. A 1 µm Z-stack of images was acquired to account for drifts and assuring the capture surface was always in focus. However, this may have led to the imaging of EVs in motion that are close to the surface and within the range of the Z-stack, but not

actually bound to an immobilized antibody. To circumvent these errors, future experiments will use smaller magnetic beads, to ensure that the focus on the beads is equivalent to the focus of only EVs bound to the surface.

Finally, in our proof-of-concept experiment, we showed that single cell studies may not need to compartmentalize cells, but rather analysis platforms can be highly simplified like the SFC. The larger surface area of the SFC enables spatial isolation of single cells. Further, the shallow chamber design and no-flow condition throughout experiments promotes the capture of diffusing EVs to the bottom capture surface and minimizes lateral diffusion of the secreted EVs. Collectively, our preliminary results demonstrate that the potentials of the developed platforms for the analysis of single secreted EVs from single cell at high temporal resolution. The unexpected dissociation of EVs to the capture surface, however, also highlight the challenges in time course analysis of EV secretion and several aspects of this work.

Future directions

While the utility of the platform was demonstrated for single cell single EV secretion analysis, addressing the challenges mentioned throughout is paramount for the applicability of the platform for biological samples. The next steps for this work are to (i) perform additional control experiments to characterize EV binding, (ii) explore different chemistries to promote covalent binding of EVs to the capture surface, (iii) extend the length of secretion experiments beyond 2 h, and (iv) use the platform for biological experiments. First, the binding affinity of different antibodies should be characterized to determine whether a capture surface with a single species of antibody will be more effective for single EV capture. For control, biotinylated EVs and an

immobilized streptavidin capture surface can be employed. Biotinylation is a widely used strategy for engineering the surface of cells and EVs and can be leveraged for quantification based on the high affinity between streptavidin and biotin[202,203]. As the association and disassociation constants for biotin-streptavidin interactions are well known, they can serve as the baseline for which EV-antibody binding can be compared.

Alternatively, we can aim to eliminate EV dissociation all together by exploring methods to bind EVs more robustly to the surface, beyond the use of antibodies. Several recent studies have attempted to shift to the use of "universal" EV markers, such as the lipid membrane, and covalent interactions via click chemistry. A promising approach that could be incorporated in our platform is the use of amphipathic peptides, amino acid sequences that reportedly binds to highly curved lipid nanovesicles, including EVs[204,205]. Peptides are covalently immobilized on a surface in a click-type reaction via copper catalyzed azide-alkyne cycloaddition (CuAAC)[205]. The highly curved EV membrane approaches the specifically designed and synthesized amphipathic peptide through electrostatic forces. The peptide is subsequently inserted into lipid-packing defects, resulting in a robust binding of EVs stabilized by peptide folding within the membrane and facilitated by the presence of hydrophobic groups[205]. Another approach could explore modifying the EV membrane itself with click chemistry moieties via metabolic labeling techniques. L-azidohomoalanine (AHA) contains a modified azido moiety that can be fed to cells in culture to incorporate into proteins during active protein synthesis[206,207]. Proteins that are incorporated within the EV membrane should therefore also express the modified azido element. Used in conjunction with a capture surface immobilized with biotin alkyne able to detect the azido-modified protein, covalent capture of EVs can be achieved[206]. The use of click chemistry for secretion dynamics

studies will, however, be limited by labeling efficiency of the chemical methods. Without a sufficiently high labeling efficiency, secreted EVs will remain undetected, and the determined secretion rate will be underestimated. Nevertheless, proper optimization of these platform modifications preventing the disassociation of capture EVs could be essential to the use of the platform for dynamic rate of secretion analysis of cell secreted EVs.

A natural extension of this work would be to use the platform for the analysis of biological samples and compare the rate of EV secretions of single cells in different environments. Hypoxia is a common feature of tumor microenvironments due to abnormal vascularization and poor blood supply and has been associated with tumor progression[208,209]. In breast cancer, hypoxia-induced EV release has been suggested to be a cause of malignant transformation[210]. Time course experiments have shown enhanced EV secretion after 24 h following the onset of hypoxia in various cell types[172,173]. With our developed platform, quantification and proteomic analysis of hypoxia induced single EVs from single cells can also be investigated at much higher temporal resolution. Cells can be cultured in hypoxic media prior to seeding and further maintained in a hypoxic environment while in the flow cell. As their secretions are imaged below, EV secretion dynamics and abundance will be compared to healthy cells. Ultimately, we can further isolate hypoxia induced EVs and deduce their potential role as non-invasive biomarkers for diseases.

6. Conclusion

In summary, we presented the design, fabrication, characterization, and analysis capabilities of single-cell platforms that enable visualization of secreted single EVs at a high temporal resolution. The platforms described herein are, to the best of our knowledge, the first to report a combination of (i) single cell isolation, (ii) detection of EVs secreted directly from single cells at a single particle resolution, and (iii) quantification of secretion dynamics at 15 min time intervals. Isolation of cells was achieved by either compartmentalization or by spatial isolation and their long-term culture within the platform supported by media perfusion and nutrient replenishment was validated. Combining the cell isolation portion with a glass EV capture surface and confocal imaging then enables the time course detection and counting of endogenously labeled single EVs truly secreted by single cells. We demonstrate the platform's ability to capture and detect first bulk purified EV populations, then EVs secreted directly from cells cultured in the platform. Proof-of-concept experiments shows that our platform could be well suited for studying cellular responses to dynamic stimuli. Secretion imaging from a single cell was achieved on the scale of minutes and a secretion rate of approximately 10 EVs/h was derived. Imaging, however, indicated a high degree of EV unbinding that could result in the repeated binding of EVs, and thus a misrepresentation of the true EV secretion rate. As such, future improvements for our platforms include modifications to the capture surface for more robust EV affinity, which will allow the monitoring of EV secretion dynamics in parallel to cell environmental changes. The ability to monitor rates of secretion and future downstream phenotyping of single EVs secreted from single cells will allow us to uncover the heterogeneity of EVs and cell to cell communication at the single cell level.

7. References

1. Liu, C. *et al.* Single-Exosome-Counting Immunoassays for Cancer Diagnostics. (2018) doi:10.1021/acs.nanolett.8b01184.
2. Abhange, K. *et al.* Small extracellular vesicles in cancer. *Bioact Mater* **6**, 3705–3743 (2021).
3. Liu, S. Y., Liao, Y., Hosseinifard, H., Imani, S. & Wen, Q. L. Diagnostic Role of Extracellular Vesicles in Cancer: A Comprehensive Systematic Review and Meta-Analysis. *Front Cell Dev Biol* **9**, 2749 (2021).
4. Urabe, F. *et al.* Extracellular vesicles as biomarkers and therapeutic targets for cancer. *Am J Physiol Cell Physiol* **318**, C29–C39 (2020).
5. Lane, R. E., Korbie, D., Hill, M. M. & Trau, M. Extracellular vesicles as circulating cancer biomarkers: opportunities and challenges. *Clin Transl Med* **7**, 14 (2018).
6. Colombo, M., Raposo, G. & Théry, C. Biogenesis, secretion, and intercellular interactions of exosomes and other extracellular vesicles. *Annu Rev Cell Dev Biol* **30**, 255–289 (2014).
7. Kowal, J. *et al.* Proteomic comparison defines novel markers to characterize heterogeneous populations of extracellular vesicle subtypes. *Proc Natl Acad Sci U S A* **113**, E968–E977 (2016).
8. Willms, E., Cabañas, C., Mäger, I., Wood, M. J. A. & Vader, P. Extracellular vesicle heterogeneity: Subpopulations, isolation techniques, and diverse functions in cancer progression. *Frontiers in Immunology* vol. 9 1 Preprint at https://doi.org/10.3389/fimmu.2018.00738 (2018).
9. Yáñez-Mó, M. *et al.* Biological properties of extracellular vesicles and their physiological functions. *J Extracell Vesicles* **4**, 1–60 (2015).
10. Booth, A. M. *et al.* Exosomes and HIV Gag bud from endosome-like domains of the T cell plasma membrane. *J Cell Biol* **172**, 923–935 (2006).
11. Skog, J. *et al.* Glioblastoma microvesicles transport RNA and proteins that promote tumour growth and provide diagnostic biomarkers. *Nat Cell Biol* **10**, 1470–1476 (2008).
12. Théry, C. *et al.* Minimal information for studies of extracellular vesicles 2018 (MISEV2018): a position statement of the International Society for Extracellular Vesicles and update of the MISEV2014 guidelines. *https://doi.org/10.1080/20013078.2018.1535750* **7**, (2018).
13. Dang, X. T. T., Kavishka, J. M., Zhang, D. X., Pirisinu, M. & Le, M. T. N. Extracellular Vesicles as an Efficient and Versatile System for Drug Delivery. *Cells 2020, Vol. 9, Page 2191* **9**, 2191 (2020).
14. Almeria, C., Kreß, S., Weber, V., Egger, D. & Kasper, C. Heterogeneity of mesenchymal stem cell-derived extracellular vesicles is highly impacted by the tissue/cell source and culture conditions. *Cell & Bioscience 2022 12:1* **12**, 1–15 (2022).
15. Akers, J. C., Gonda, D., Kim, R., Carter, B. S. & Chen, C. C. Biogenesis of extracellular vesicles (EV): exosomes, microvesicles, retrovirus-like vesicles, and apoptotic bodies. *J Neurooncol* **113**, 1 (2013).
16. Atkin-Smith, G. K. & Poon, I. K. H. Disassembly of the Dying: Mechanisms and Functions. *Trends Cell Biol* **27**, 151–162 (2017).
17. Elmore, S. Apoptosis: a review of programmed cell death. *Toxicol Pathol* **35**, 495–516 (2007).
18. Kalra, H., Drummen, G. P. C. & Mathivanan, S. Focus on Extracellular Vesicles: Introducing the Next Small Big Thing. *Int J Mol Sci* **17**, (2016).
19. Théry, C. *et al.* Proteomic analysis of dendritic cell-derived exosomes: a secreted subcellular compartment distinct from apoptotic vesicles. *J Immunol* **166**, 7309–7318 (2001).

20. Escrevente, C., Keller, S., Altevogt, P. & Costa, J. Interaction and uptake of exosomes by ovarian cancer cells. *BMC Cancer* **11**, 1–10 (2011).
21. Samanta, S. *et al.* Exosomes: new molecular targets of diseases. *Acta Pharmacologica Sinica 2018 39:4* **39**, 501–513 (2017).
22. Hugel, B., Martínez, M. C., Kunzelmann, C. & Freyssinet, J. M. Membrane microparticles: Two sides of the coin. *Physiology* **20**, 22–27 (2005).
23. Doyle, L. M. & Wang, M. Z. Overview of Extracellular Vesicles, Their Origin, Composition, Purpose, and Methods for Exosome Isolation and Analysis. *Cells* **8**, (2019).
24. Veerman, R. E. *et al.* Molecular evaluation of five different isolation methods for extracellular vesicles reveals different clinical applicability and subcellular origin. *J Extracell Vesicles* **10**, e12128 (2021).
25. White, I. J., Bailey, L. M., Aghakhani, M. R., Moss, S. E. & Futter, C. E. EGF stimulates annexin 1-dependent inward vesiculation in a multivesicular endosome subpopulation. *EMBO J* **25**, 1–12 (2006).
26. Harding, C. v., Heuser, J. E. & Stahl, P. D. Exosomes: Looking back three decades and into the future. *J Cell Biol* **200**, 367 (2013).
27. van Niel, G., D'Angelo, G. & Raposo, G. Shedding light on the cell biology of extracellular vesicles. *Nature Reviews Molecular Cell Biology 2018 19:4* **19**, 213–228 (2018).
28. Minciacchi, V. R. *et al.* Large oncosomes contain distinct protein cargo and represent a separate functional class of tumor-derived extracellular vesicles. *Oncotarget* **6**, 11327 (2015).
29. Jaiswal, R. & Sedger, L. M. Intercellular vesicular transfer by exosomes, microparticles and oncosomes - Implications for cancer biology and treatments. *Front Oncol* **9**, 125 (2019).
30. Ciardiello, C. *et al.* Large oncosomes overexpressing integrin alpha-V promote prostate cancer adhesion and invasion via AKT activation. *Journal of Experimental and Clinical Cancer Research* **38**, 1–16 (2019).
31. Wollert, T. & Hurley, J. H. Molecular Mechanism of Multivesicular Body Biogenesis by ESCRT Complexes. *Nature* **464**, 864 (2010).
32. Hurley, J. H. & Hanson, P. I. Membrane budding and scission by the ESCRT machinery: it's all in the neck. *Nat Rev Mol Cell Biol* **11**, 556–566 (2010).
33. Fang, Y. *et al.* Higher-order oligomerization targets plasma membrane proteins and HIV Gag to exosomes. *PLoS Biol* **5**, 1267–1283 (2007).
34. Trajkovic, K. *et al.* Ceramide triggers budding of exosome vesicles into multivesicular endosomes. *Science* **319**, 1244–1247 (2008).
35. Costa-Silva, B. *et al.* Pancreatic cancer exosomes initiate pre-metastatic niche formation in the liver. *Nat Cell Biol* **17**, 816 (2015).
36. Xiao, D. *et al.* Melanoma cell-derived exosomes promote epithelial-mesenchymal transition in primary melanocytes through paracrine/autocrine signaling in the tumor microenvironment. *Cancer Lett* **376**, 318–327 (2016).
37. Antonyak, M. A. *et al.* Cancer cell-derived microvesicles induce transformation by transferring tissue transglutaminase and fibronectin to recipient cells. *Proc Natl Acad Sci U S A* **108**, 4852–4857 (2011).
38. Xu, R. *et al.* Extracellular vesicles in cancer — implications for future improvements in cancer care. *Nature Reviews Clinical Oncology* vol. 15 617–638 Preprint at https://doi.org/10.1038/s41571-018-0036-9 (2018).

39. Jeong, W. K. *et al.* Fas Ligand–Positive Membranous Vesicles Isolated from Sera of Patients with Oral Cancer Induce Apoptosis of Activated T Lymphocytes. *Clinical Cancer Research* **11**, 1010–1020 (2005).
40. Wieckowski, E. U. *et al.* Tumor-derived microvesicles promote regulatory T cell expansion and induce apoptosis in tumor-reactive activated CD8+ T lymphocytes. *J Immunol* **183**, 3720–3730 (2009).
41. Han, L., Lam, E. W. F. & Sun, Y. Extracellular vesicles in the tumor microenvironment: old stories, but new tales. *Molecular Cancer 2019 18:1* **18**, 1–14 (2019).
42. Kucharzewska, P. *et al.* Exosomes reflect the hypoxic status of glioma cells and mediate hypoxia-dependent activation of vascular cells during tumor development. *Proc Natl Acad Sci U S A* **110**, 7312–7317 (2013).
43. Umezu, T. *et al.* Exosomal miR-135b shed from hypoxic multiple myeloma cells enhances angiogenesis by targeting factor-inhibiting HIF-1. *Blood* **124**, 3748–3757 (2014).
44. Chaffer, C. L. & Weinberg, R. A. A perspective on cancer cell metastasis. *Science (1979)* **331**, 1559–1564 (2011).
45. Peinado, H. *et al.* Pre-metastatic niches: organ-specific homes for metastases. *Nat Rev Cancer* **17**, 302–317 (2017).
46. Psaila, B. & Lyden, D. The Metastatic Niche: Adapting the Foreign Soil. *Nat Rev Cancer* **9**, 285 (2009).
47. Lobb, R. J., Lima, L. G. & Möller, A. Exosomes: Key mediators of metastasis and pre-metastatic niche formation. *Seminars in Cell and Developmental Biology* vol. 67 3–10 Preprint at https://doi.org/10.1016/j.semcdb.2017.01.004 (2017).
48. Fong, M. Y. *et al.* Breast-cancer-secreted miR-122 reprograms glucose metabolism in premetastatic niche to promote metastasis. *Nat Cell Biol* **17**, 183–194 (2015).
49. Vasconcelos, M. H., Caires, H. R., Ābols, A., Xavier, C. P. R. & Linē, A. Extracellular vesicles as a novel source of biomarkers in liquid biopsies for monitoring cancer progression and drug resistance. *Drug Resistance Updates* **47**, 100647 (2019).
50. Nannan, L. *et al.* Extracellular Vesicle-Dependent Cross-Talk in Cancer—Focus on Pancreatic Cancer. *Front Oncol* **10**, 1456 (2020).
51. Bebelman, M. P., Janssen, E., Pegtel, D. M. & Crudden, C. The forces driving cancer extracellular vesicle secretion. *Neoplasia* **23**, 149 (2021).
52. Amintas, S. *et al.* Next-Generation Cancer Biomarkers: Extracellular Vesicle DNA as a Circulating Surrogate of Tumor DNA. *Front Cell Dev Biol* **8**, 1806 (2021).
53. Huang, G., Lin, G., Zhu, Y., Duan, W. & Jin, D. Emerging technologies for profiling extracellular vesicle heterogeneity. *Lab Chip* **20**, 2423–2437 (2020).
54. Roy, S. *et al.* Navigating the Landscape of Tumor Extracellular Vesicle Heterogeneity. *International Journal of Molecular Sciences 2019, Vol. 20, Page 1349* **20**, 1349 (2019).
55. Hemler, M. E. Tetraspanin functions and associated microdomains. *Nat Rev Mol Cell Biol* **6**, 801–811 (2005).
56. Jankovičová, J., Sečová, P., Michalková, K. & Antalíková, J. Tetraspanins, More than Markers of Extracellular Vesicles in Reproduction. *Int J Mol Sci* **21**, 1–30 (2020).
57. Hurwitz, S. N. & Meckes, D. G. Extracellular Vesicle Integrins Distinguish Unique Cancers. *Proteomes* **7**, (2019).
58. Nolte, M. A., Nolte-'t Hoen, E. N. M. & Margadant, C. Integrins Control Vesicular Trafficking; New Tricks for Old Dogs. *Trends Biochem Sci* **46**, 124 (2021).

59. Fernanda Altei, W. *et al.* Extracellular Vesicles and Integrins: Partners in Cancer Progression. *Role of Exosomes in Biological Communication Systems* 293–310 (2021) doi:10.1007/978-981-15-6599-1_14.
60. Melo, S. A. *et al.* Glypican1 identifies cancer exosomes and facilitates early detection of cancer. *Nature* **523**, 177 (2015).
61. Guan, M. *et al.* MDA-9 and GRP78 as potential diagnostic biomarkers for early detection of melanoma metastasis. *Tumor Biology* **36**, 2973–2982 (2015).
62. Peinado, H. *et al.* Melanoma exosomes educate bone marrow progenitor cells toward a pro-metastatic phenotype through MET. *Nature Medicine 2012 18:6* **18**, 883–891 (2012).
63. Moon, P. G. *et al.* Identification of developmental endothelial locus-1 on circulating extracellular vesicles as a novel biomarker for early breast cancer detection. *Clinical Cancer Research* **22**, 1757–1766 (2016).
64. Kibria, G. *et al.* A rapid, automated surface protein profiling of single circulating exosomes in human blood. *Scientific Reports 2016 6:1* **6**, 1–9 (2016).
65. Fang, S. *et al.* Clinical application of a microfluidic chip for immunocapture and quantification of circulating exosomes to assist breast cancer diagnosis and molecular classification. *PLoS One* **12**, (2017).
66. Kwizera, E. A. *et al.* Molecular Detection and Analysis of Exosomes Using Surface-Enhanced Raman Scattering Gold Nanorods and a Miniaturized Device. *Theranostics* **8**, 2722 (2018).
67. Cui, Z. *et al.* Diagnostic and prognostic value of the cancer-testis antigen lactate dehydrogenase C4 in breast cancer. *Clinica Chimica Acta* **503**, 203–209 (2020).
68. Hoshino, A. *et al.* Tumour exosome integrins determine organotropic metastasis. *Nature* **527**, 329–335 (2015).
69. Tao, S. C. & Guo, S. C. Role of extracellular vesicles in tumour microenvironment. *Cell Communication and Signaling 2020 18:1* **18**, 1–24 (2020).
70. Chang, W. H., Cerione, R. A. & Antonyak, M. A. Extracellular Vesicles and Their Roles in Cancer Progression. *Methods Mol Biol* **2174**, 143 (2021).
71. Becker, A. *et al.* Extracellular vesicles in cancer: cell-to-cell mediators of metastasis. *Cancer Cell* **30**, 836 (2016).
72. Kosaka, N., Yoshioka, Y., Fujita, Y. & Ochiya, T. Versatile roles of extracellular vesicles in cancer. *J Clin Invest* **126**, 1163–1172 (2016).
73. Macklin, A., Khan, S. & Kislinger, T. Recent advances in mass spectrometry based clinical proteomics: applications to cancer research. *Clinical Proteomics 2020 17:1* **17**, 1–25 (2020).
74. Beck, L. & Geiger, T. MS-based technologies for untargeted single-cell proteomics. *Curr Opin Biotechnol* **76**, 102736 (2022).
75. Klymus, K. E. *et al.* Reporting the limits of detection and quantification for environmental DNA assays. *Environmental DNA* **2**, 271–282 (2020).
76. Xiong, Y., Leng, Y., Li, X., Huang, X. & Xiong, Y. Emerging strategies to enhance the sensitivity of competitive ELISA for detection of chemical contaminants in food samples. *TrAC Trends in Analytical Chemistry* **126**, 115861 (2020).
77. Yang, Z. *et al.* Ultrasensitive Single Extracellular Vesicle Detection Using High Throughput Droplet Digital Enzyme-Linked Immunosorbent Assay. *Cite This: Nano Lett* **2022**, 4315–4324 (2022).
78. Zhang, P., He, M. & Zeng, Y. Ultrasensitive microfluidic analysis of circulating exosomes using a nanostructured graphene oxide/polydopamine coating. *Lab Chip* **16**, 3033–3042 (2016).

79. Vaidyanathan, R. *et al.* Detecting exosomes specifically: A multiplexed device based on alternating current electrohydrodynamic induced nanoshearing. *Anal Chem* **86**, 11125–11132 (2014).
80. Ishihara, R. *et al.* Design of a Sensitive Extracellular Vesicle Detection Method Utilizing a Surface-Functionalized Power-Free Microchip. *Membranes (Basel)* **12**, (2022).
81. Borges, F. T., Reis, L. A. & Schor, N. Extracellular vesicles: structure, function, and potential clinical uses in renal diseases. *Brazilian Journal of Medical and Biological Research* **46**, 824 (2013).
82. He, C., Wang, L., Li, L. & Zhu, G. Extracellular vesicle-orchestrated crosstalk between cancer-associated fibroblasts and tumors. *Transl Oncol* **14**, 101231 (2021).
83. Burbidge, K. *et al.* Cargo and cell-specific differences in extracellular vesicle populations identified by multiplexed immunofluorescent analysis. *J Extracell Vesicles* **9**, 1789326 (2020).
84. Panagopoulou, M. S., Wark, A. W., Birch, D. J. S. & Gregory, C. D. Phenotypic analysis of extracellular vesicles: a review on the applications of fluorescence. *J Extracell Vesicles* **9**, 1710020 (2020).
85. Dagher, M., Kleinman, M., Ng, A. & Juncker, D. Ensemble multicolour FRET model enables barcoding at extreme FRET levels. *Nat Nanotechnol* **13**, 925–932 (2018).
86. Rothenberg, D. A. *et al.* A Proteomics Approach to Profiling the Temporal Translational Response to Stress and Growth. *iScience* **9**, 367–381 (2018).
87. Golan-Lavi, R. *et al.* Coordinated Pulses of mRNA and of Protein Translation or Degradation Produce EGF-Induced Protein Bursts. *Cell Rep* **18**, 3129–3142 (2017).
88. Zhang, Z. *et al.* A High-Temporal Resolution Technology for Dynamic Proteomic Analysis Based on 35S Labeling. *PLoS One* **3**, 2991 (2008).
89. Rahmatbakhsh, M., Gagarinova, A. & Babu, M. Bioinformatic Analysis of Temporal and Spatial Proteome Alternations During Infections. *Front Genet* **12**, 1155 (2021).
90. Shirasaki, Y. *et al.* Real-time single-cell imaging of protein secretion. *Sci Rep* **4**, 1–8 (2014).
91. Sina, A. A. I. *et al.* Real time and label free profiling of clinically relevant exosomes. *Sci Rep* **6**, (2016).
92. Cai, W. *et al.* A single-cell translocation and secretion assay (TransSeA). *Lab Chip* **18**, 3154–3162 (2018).
93. Chiu, Y. J., Cai, W., Shih, Y. R. v., Lian, I. & Lo, Y. H. A Single-Cell Assay for Time Lapse Studies of Exosome Secretion and Cell Behaviors. *Small* **12**, 3658–3666 (2016).
94. Zhu, F. *et al.* High-Throughput Single-Cell Extracellular Vesicle Secretion Analysis on a Desktop Scanner without Cell Counting. *Anal Chem* **93**, 13152–13160 (2021).
95. Wen, Y. *et al.* Factors influencing the measurement of the secretion rate of extracellular vesicles. *Analyst* **145**, 5870–5877 (2020).
96. Wang, J. & Fleischmann, D. Improving Spatial Resolution at CT: Development, Benefits, and Pitfalls. *https://doi.org/10.1148/radiol.2018181156* **289**, 261–262 (2018).
97. Jørgensen, M. *et al.* Extracellular Vesicle (EV) Array: microarray capturing of exosomes and other extracellular vesicles for multiplexed phenotyping. *J Extracell Vesicles* **2**, (2013).
98. Martel, R., Shen, M. L., DeCorwin-Martin, P., Araujo, L. O. F. de & Juncker, D. Extracellular Vesicle Antibody Microarray for Multiplexed Inner and Outer Protein Analysis. *bioRxiv* 2022.04.05.487234 (2022) doi:10.1101/2022.04.05.487234.
99. Rissin, D. M. *et al.* Multiplexed single molecule immunoassays. *Lab Chip* **13**, 2902–2911 (2013).

100. Chiang, C. Y. & Chen, C. Toward characterizing extracellular vesicles at a single-particle level Tse-Hua Tan. *Journal of Biomedical Science* vol. 26 9 Preprint at https://doi.org/10.1186/s12929-019-0502-4 (2019).
101. van der Pol, E. *et al.* Optical and non-optical methods for detection and characterization of microparticles and exosomes. *Journal of Thrombosis and Haemostasis* **8**, 2596–2607 (2010).
102. Brittain, G. C. *et al.* A Novel Semiconductor-Based Flow Cytometer with Enhanced Light-Scatter Sensitivity for the Analysis of Biological Nanoparticles. *Scientific Reports 2019 9:1* **9**, 1–13 (2019).
103. Salmond, N., Khanna, K., Owen, G. R. & Williams, K. C. Nanoscale flow cytometry for immunophenotyping and quantitating extracellular vesicles in blood plasma. *Nanoscale* **13**, 2012–2025 (2021).
104. Mizenko, R. R. *et al.* Tetraspanins are unevenly distributed across single extracellular vesicles and bias sensitivity to multiplexed cancer biomarkers. *J Nanobiotechnology* **19**, 1–17 (2021).
105. Breitwieser, K. *et al.* Detailed Characterization of Small Extracellular Vesicles from Different Cell Types Based on Tetraspanin Composition by ExoView R100 Platform. *Int J Mol Sci* **23**, (2022).
106. Lee, K. *et al.* Multiplexed Profiling of Single Extracellular Vesicles. (2017) doi:10.1021/acsnano.7b07060.
107. Han, C. *et al.* Single-vesicle imaging and co-localization analysis for tetraspanin profiling of individual extracellular vesicles. *J Extracell Vesicles* **10**, (2021).
108. Ferguson, S. *et al.* Single-EV analysis (sEVA) of mutated proteins allows detection of stage 1 pancreatic cancer. *Sci Adv* **8**, (2022).
109. Verweij, F. J. *et al.* The power of imaging to understand extracellular vesicle biology in vivo. *Nat Methods* **18**, 1013 (2021).
110. Lai, C. P. *et al.* Visualization and tracking of tumour extracellular vesicle delivery and RNA translation using multiplexed reporters. *Nat Commun* **6**, (2015).
111. Ortega Arroyo, J., Cole, D. & Kukura, P. Interferometric scattering microscopy and its combination with single-molecule fluorescence imaging. *Nature Protocols 2016 11:4* **11**, 617–633 (2016).
112. Mcdonald, M. P. *et al.* Visualizing Single-Cell Secretion Dynamics with Single-Protein Sensitivity. (2018) doi:10.1021/acs.nanolett.7b04494.
113. Dehghani, M., Gulvin, S. M., Flax, J. & Gaborski, T. R. Systematic Evaluation of PKH Labelling on Extracellular Vesicle Size by Nanoparticle Tracking Analysis. *Scientific Reports 2020 10:1* **10**, 1–10 (2020).
114. Simonsen, J. B. Pitfalls associated with lipophilic fluorophore staining of extracellular vesicles for uptake studies. *J Extracell Vesicles* **8**, (2019).
115. Jung, K. O. *et al.* Visualization of exosome-mediated miR-210 transfer from hypoxic tumor cells. *Oncotarget* **8**, 9899–9910 (2016).
116. Watson, D. C. *et al.* Efficient production and enhanced tumor delivery of engineered extracellular vesicles. *Biomaterials* **105**, 195–205 (2016).
117. Lai, C. P. *et al.* Dynamic Biodistribution of Extracellular Vesicles In Vivo Using a Multimodal Imaging Reporter. *ACS Nano* **8**, 483 (2014).
118. Ender, F., Zamzow, P., von Bubnoff, N. & Gieseler, F. Detection and Quantification of Extracellular Vesicles via FACS: Membrane Labeling Matters! *Int J Mol Sci* **21**, (2020).
119. Morales-Kastresana, A. *et al.* Labeling Extracellular Vesicles for Nanoscale Flow Cytometry. *Scientific Reports 2017 7:1* **7**, 1–10 (2017).

120. Chuo, S. T. Y., Chien, J. C. Y. & Lai, C. P. K. Imaging extracellular vesicles: Current and emerging methods. *J Biomed Sci* **25**, 1–10 (2018).

121. He, D. *et al.* Total internal reflection-based single-vesicle in situ quantitative and stoichiometric analysis of tumor-derived exosomal microRNAs for diagnosis and treatment monitoring. *Theranostics* **9**, 4494 (2019).

122. Nikoloff, J. M., Saucedo-Espinosa, M. A., Kling, A. & Dittrich, P. S. Identifying extracellular vesicle populations from single cells. *Proc Natl Acad Sci U S A* **118**, (2021).

123. Nizamudeen, Z. *et al.* Rapid and accurate analysis of stem cell-derived extracellular vesicles with super resolution microscopy and live imaging. *Biochim Biophys Acta Mol Cell Res* **1865**, 1891 (2018).

124. Lai, C. P. *et al.* Visualization and tracking of tumour extracellular vesicle delivery and RNA translation using multiplexed reporters. *Nature Communications 2015 6:1* **6**, 1–12 (2015).

125. Yim, N. *et al.* Exosome engineering for efficient intracellular delivery of soluble proteins using optically reversible protein–protein interaction module. *Nature Communications 2016 7:1* **7**, 1–9 (2016).

126. Stickney, Z., Losacco, J., McDevitt, S., Zhang, Z. & Lu, B. Development of exosome surface display technology in living human cells. *Biochem Biophys Res Commun* **472**, 53–59 (2016).

127. Levy, D. *et al.* Genetic labeling of extracellular vesicles for studying biogenesis and uptake in living mammalian cells. *Methods Enzymol* **645**, 1–14 (2020).

128. Sandoghdar, V., Stoller, P., Vogel, V., Jacobsen, V. & Brunner, C. Interferometric optical detection and tracking of very small gold nanoparticles at a water-glass interface. *Optics Express, Vol. 14, Issue 1, pp. 405-414* **14**, 405–414 (2006).

129. Lindfors, K., Kalkbrenner, T., Stoller, P. & Sandoghdar, V. Detection and Spectroscopy of Gold Nanoparticles Using Supercontinuum White Light Confocal Microscopy. doi:10.1103/PhysRevLett.93.037401.

130. Gemeinhardt, A. *et al.* Label-free imaging of single proteins secreted from living cells via iscat microscopy. *Journal of Visualized Experiments* **2018**, 58486 (2018).

131. Piliarik, M. & Sandoghdar, V. Direct optical sensing of single unlabelled proteins and super-resolution imaging of their binding sites. *Nature Communications 2014 5:1* **5**, 1–8 (2014).

132. Bucheli, O. T. M., Sigvaldadóttir, I. & Eyer, K. Measuring single-cell protein secretion in immunology: Technologies, advances, and applications. *Eur J Immunol* **51**, 1334–1347 (2021).

133. Lu, Y. *et al.* Highly multiplexed profiling of single-cell effector functions reveals deep functional heterogeneity in response to pathogenic ligands. *Proc Natl Acad Sci U S A* **112**, E607–E615 (2015).

134. Chokkalingam, V. *et al.* Probing cellular heterogeneity in cytokine-secreting immune cells using droplet-based microfluidics. *Lab Chip* **13**, 4740–4744 (2013).

135. Altschuler, S. J. & Wu, L. F. Cellular heterogeneity: when do differences make a difference? *Cell* **141**, 559 (2010).

136. Dagogo-Jack, I. & Shaw, A. T. Tumour heterogeneity and resistance to cancer therapies. *Nature Reviews Clinical Oncology 2017 15:2* **15**, 81–94 (2017).

137. Landau, D. A. *et al.* Evolution and impact of subclonal mutations in chronic lymphocytic leukemia. *Cell* **152**, 714–726 (2013).

138. Chen, Z., Chen, J. J. & Fan, R. Single-Cell Protein Secretion Detection and Profiling. *Annual Review of Analytical Chemistry* **11**, 18 (2019).

139. Xie, H. & Ding, X. The Intriguing Landscape of Single-Cell Protein Analysis. *Advanced Science* **9**, 2105932 (2022).

140. Schmid, A., Kortmann, H., Dittrich, P. S. & Blank, L. M. Chemical and biological single cell analysis. *Curr Opin Biotechnol* **21**, 12–20 (2010).
141. Xu, B., Du, W., Liu, B.-F. & Luo, Q. Single Cell Proteomics: Challenge for Current Analytical Science. *Curr Anal Chem* **2**, 67–76 (2005).
142. Levy, E. & Slavov, N. Single cell protein analysis for systems biology. *Essays Biochem* **62**, 595 (2018).
143. Slavov, N. Unpicking the proteome in single cells:: Single-cell mass spectrometry will help reveal mechanisms that underpin health and disease. *Science* **367**, 512 (2020).
144. Saadatpour, A., Lai, S., Guo, G. & Yuan, G. C. Single-cell analysis in cancer genomics. *Trends Genet* **31**, 576 (2015).
145. Slota, M., Lim, J. B., Dang, Y. & Disis, M. L. ELISpot for measuring human immune responses to vaccines. *Expert Rev Vaccines* **10**, 299 (2011).
146. Janetzki, S. & Rabin, R. Enzyme-linked immunospot (Elispot) for single-cell analysis. *Methods in Molecular Biology* **1346**, 27–46 (2015).
147. Eyer, K. *et al.* Single-cell deep phenotyping of IgG-secreting cells for high-resolution immune monitoring. *Nature Biotechnology 2017 35:10* **35**, 977–982 (2017).
148. Boulet, S. *et al.* A Dual Color ELISPOT Method for the Simultaneous Detection of IL-2 and IFN-γ HIV-Specific Immune Responses. *J Immunol Methods* **320**, 18 (2007).
149. Janetzki, S., Rueger, M. & Dillenbeck, T. Stepping up ELISpot: Multi-Level Analysis in FluoroSpot Assays. *Cells* **3**, 1102 (2014).
150. Körber, N., Behrends, U., Hapfelmeier, A., Protzer, U. & Bauer, T. Validation of an IFNγ/IL2 FluoroSpot assay for clinical trial monitoring. *J Transl Med* **14**, 1–12 (2016).
151. Yuan, J. & Sims, P. A. An Automated Microwell Platform for Large-Scale Single Cell RNA-Seq. *Scientific Reports 2016 6:1* **6**, 1–10 (2016).
152. Sandström, N. *et al.* Live single cell imaging assays in glass microwells produced by laser-induced deep etching. *Lab Chip* **22**, 2107–2121 (2022).
153. Liu, Y. & Singh, A. K. Microfluidic Platforms for Single-Cell Protein Analysis. *J Lab Autom* **18**, 446–454 (2013).
154. Han, Q., Bradshaw, E. M., Nilsson, B., Hafler, D. A. & Love, J. C. Multidimensional analysis of the frequencies and rates of cytokine secretion from single cells by quantitative microengraving. *Lab Chip* **10**, 1391–1400 (2010).
155. Love, J. C., Ronan, J. L., Grotenbreg, G. M., van der Veen, A. G. & Ploegh, H. L. A microengraving method for rapid selection of single cells producing antigen-specific antibodies. *Nature Biotechnology 2006 24:6* **24**, 703–707 (2006).
156. Swennenhuis, J. F. *et al.* Self-seeding microwell chip for the isolation and characterization of single cells. *Lab Chip* **15**, 3039–3046 (2015).
157. Collins, D. J., Neild, A., deMello, A., Liu, A. Q. & Ai, Y. The Poisson distribution and beyond: Methods for microfluidic droplet production and single cell encapsulation. *Lab on a Chip* vol. 15 3439–3459 Preprint at https://doi.org/10.1039/c5lc00614g (2015).
158. Ji, Y. *et al.* Multiplexed profiling of single-cell extracellular vesicles secretion. *Proc Natl Acad Sci U S A* **116**, 5979–5984 (2019).
159. Cai, Y. & Wu, D. High-Throughput Single Extracellular Vesicle Profiling. (2021) doi:10.5772/INTECHOPEN.97544.
160. Choi, J. R. *et al.* Monolithic hydrogel nanowells-in-microwells enabling simultaneous single cell secretion and phenotype analysis. *Lab Chip* **20**, 4539 (2020).

161. Burklund, A., Tadimety, A., Nie, Y., Hao, N. & Zhang, J. X. J. Advances in diagnostic microfluidics. *Adv Clin Chem* **95**, 1–72 (2020).
162. Whitesides, G. M. The origins and the future of microfluidics. *Nature 2006 442:7101* **442**, 368–373 (2006).
163. Shembekar, N., Chaipan, C., Utharala, R. & Merten, C. A. Droplet-based microfluidics in drug discovery, transcriptomics and high-throughput molecular genetics. *Lab Chip* **16**, 1314–1331 (2016).
164. Sukovich, D. J., Kim, S. C., Ahmed, N. & Abate, A. R. Bulk double emulsification for flow cytometric analysis of microfluidic droplets. *Analyst* **142**, 4618–4622 (2017).
165. Hilton, S. H. & White, I. M. Advances in the analysis of single extracellular vesicles: A critical review. *Sensors and Actuators Reports* **3**, 100052 (2021).
166. Zhou, J. *et al.* High-throughput single-EV liquid biopsy: Rapid, simultaneous, and multiplexed detection of nucleic acids, proteins, and their combinations. *Sci Adv* **6**, (2020).
167. Ko, J., Wang, Y., Sheng, K., Weitz, D. A. & Weissleder, R. Sequencing-Based Protein Analysis of Single Extracellular Vesicles. *ACS Nano* **15**, 5631–5638 (2021).
168. Ferguson, S. W. & Nguyen, J. Exosomes as therapeutics: The implications of molecular composition and exosomal heterogeneity. *J Control Release* **228**, 179–190 (2016).
169. Willms, E. *et al.* Cells release subpopulations of exosomes with distinct molecular and biological properties. *Scientific Reports 2016 6:1* **6**, 1–12 (2016).
170. Sawicki, L. A., Choe, L. H., Wiley, K. L., Lee, K. H. & Kloxin, A. M. Isolation and Identification of Proteins Secreted by Cells Cultured within Synthetic Hydrogel-Based Matrices. *ACS Biomater Sci Eng* **4**, 836–845 (2018).
171. Xue, Q. *et al.* Analysis of single-cell cytokine secretion reveals a role for paracrine signaling in coordinating macrophage responses to TLR4 stimulation. *Sci Signal* **8**, ra59 (2015).
172. Muñiz-García, A. *et al.* Hypoxia-induced HIF1α activation regulates small extracellular vesicle release in human embryonic kidney cells. *Scientific Reports 2022 12:1* **12**, 1–14 (2022).
173. Kilic, T., Valinhas, A. T. D. S., Wall, I., Renaud, P. & Carrara, S. Label-free detection of hypoxia-induced extracellular vesicle secretion from MCF-7 cells. *Sci Rep* **8**, 1–9 (2018).
174. Hattori, K. *et al.* Droplet Array-Based Platform for Parallel Optical Analysis of Dynamic Extracellular Vesicle Secretion from Single Cells. *Anal Chem* **94**, 11209–11215 (2022).
175. Hernández-Castro, J. A., Li, K., Meunier, A., Juncker, D. & Veres, T. Fabrication of large-area polymer microfilter membranes and their application for particle and cell enrichment. *Lab Chip* **17**, 1960–1969 (2017).
176. Beamish, J. A., Zhu, J., Kottke-Marchant, K. & Marchant, R. E. The effects of monoacrylated poly(ethylene glycol) on the properties of poly(ethylene glycol) diacrylate hydrogels used for tissue engineering. *J Biomed Mater Res A* **92A**, 441–450 (2010).
177. Rekowska, N. *et al.* Thermal, Mechanical and Biocompatibility Analyses of Photochemically Polymerized PEGDA250 for Photopolymerization-Based Manufacturing Processes. *Pharmaceutics* **14**, (2022).
178. Deng, X. *et al.* 3D printing of robust and biocompatible poly(ethylene glycol)diacrylate/nano-hydroxyapatite composites via continuous liquid interface production. *J Mater Chem B* **9**, 1315–1324 (2021).
179. Choi, J. R., Yong, K. W., Choi, J. Y. & Cowie, A. C. Recent advances in photo-crosslinkable hydrogels for biomedical applications. *Biotechniques* **66**, 40–53 (2019).

180. Kadilak, A. L., Rehaag, J. C., Harrington, C. A. & Shor, L. M. A 3D-printed microbial cell culture platform with in situ PEGDA hydrogel barriers for differential substrate delivery. doi:10.1063/1.5003477.

181. Moon, J. J., Hahn, M. S., Kim, I., Nsiah, B. A. & West, J. L. *Micropatterning of Poly(Ethylene Glycol) Diacrylate Hydrogels with Biomolecules to Regulate and Guide Endothelial Morphogenesis*.

182. Chan, V., Zorlutuna, P., Jeong, J. H., Kong, H. & Bashir, R. Three-dimensional photopatterning of hydrogels using stereolithography for long-term cell encapsulation. *Lab Chip* **10**, 2062–2070 (2010).

183. Peppas, N. A., Bures, P., Leobandung, W. & Ichikawa, H. Hydrogels in pharmaceutical formulations. *European Journal of Pharmaceutics and Biopharmaceutics* **50**, 27–46 (2000).

184. Holback, H., Yeo, Y. & Park, K. Hydrogel swelling behavior and its biomedical applications. *Biomedical Hydrogels* 3–24 (2011) doi:10.1533/9780857091383.1.3.

185. Raman, R. & Bashir, R. Stereolithographic 3D Bioprinting for Biomedical Applications. *Essentials of 3D Biofabrication and Translation* 89–121 (2015) doi:10.1016/B978-0-12-800972-7.00006-2.

186. Jachimska, B., Wasilewska, M. & Adamczyk, Z. Characterization of globular protein solutions by dynamic light scattering, electrophoretic mobility, and viscosity measurements. *Langmuir* **24**, 6867–6872 (2008).

187. Thorne, R. G., Hrabětová, S. & Nicholson, C. Diffusion of epidermal growth factor in rat brain extracellular space measured by integrative optical imaging. *J Neurophysiol* **92**, 3471–3481 (2004).

188. Lee, Y. M. & Kim, S. Y. Stimuli-responsive interpenetrating polymer network hydrogels composed of poly(vinyl alcohol) and poly(acrylic acid). *Smart Fibres, Fabrics and Clothing* 93–108 (2001) doi:10.1533/9781855737600.93.

189. Armstrong, J. K., Wenby, R. B., Meiselman, H. J. & Fisher, T. C. The Hydrodynamic Radii of Macromolecules and Their Effect on Red Blood Cell Aggregation. *Biophys J* **87**, 4259 (2004).

190. Zhang, C., Hekmatfer, S. & Karuri, N. W. A comparative study of polyethylene glycol hydrogels derivatized with the RGD peptide and the cell-binding domain of fibronectin. *J Biomed Mater Res A* **102**, 170–179 (2014).

191. Munoz-Pinto, D. J., Jimenez-Vergara, A. C., Gharat, T. P. & Hahn, M. S. Characterization of sequential collagen-poly(ethylene glycol) diacrylate interpenetrating networks and initial assessment of their potential for vascular tissue engineering. *Biomaterials* **40**, 32–42 (2015).

192. Zhu, J. Bioactive modification of poly(ethylene glycol) hydrogels for tissue engineering. *Biomaterials* **31**, 4639–4656 (2010).

193. Wang, Y. *et al.* ECM proteins in a microporous scaffold influence hepatocyte morphology, function, and gene expression. *Scientific Reports 2016 6:1* **6**, 1–13 (2016).

194. Tanyeri, M. & Tay, S. Viable cell culture in PDMS-based microfluidic devices. *Methods Cell Biol* **148**, 3–33 (2018).

195. Chumbimuni-Torres, K. Y. *et al.* Adsorption of Proteins to Thin-Films of PDMS and Its Effect on the Adhesion of Human Endothelial Cells. *RSC Adv* **1**, 706–714 (2011).

196. Spuul, P., Chi, P. Y., Billottet, C., Chou, C. F. & Génot, E. Microfluidic devices for the study of actin cytoskeleton in constricted environments: Evidence for podosome formation in endothelial cells exposed to a confined slit. *Methods* **94**, 65–74 (2016).

197. Cornelissen, C. G. *et al.* Fibronectin coating of oxygenator membranes enhances endothelial cell attachment. *Biomed Eng Online* **12**, 7 (2013).

198. Kumra Ahnlide, V., de Neergaard, T., Sundwall, M., Ambjörnsson, T. & Nordenfelt, P. A Predictive Model of Antibody Binding in the Presence of IgG-Interacting Bacterial Surface Proteins. *Front Immunol* **12**, 661 (2021).
199. Moon, P. G. *et al.* Fibronectin on circulating extracellular vesicles as a liquid biopsy to detect breast cancer. *Oncotarget* **7**, 40189 (2016).
200. Sung, B. H., Ketova, T., Hoshino, D., Zijlstra, A. & Weaver, A. M. Directional cell movement through tissues is controlled by exosome secretion. *Nat Commun* **6**, (2015).
201. Purushothaman, A. *et al.* Fibronectin on the Surface of Myeloma Cell-derived Exosomes Mediates Exosome-Cell Interactions. *J Biol Chem* **291**, 1652 (2016).
202. Dong, D., Zhu, L., Hu, J., Pang, D. W. & Zhang, Z. L. Simple and rapid extracellular vesicles quantification via membrane biotinylation strategy coupled with fluorescent nanospheres-based lateral flow assay. *Talanta* **200**, 408–414 (2019).
203. Kang, Y. T. *et al.* Multiplex Isolation and Profiling of Extracellular Vesicles using a Microfluidic DICE Device. *Analyst* **144**, 5785 (2019).
204. Saludes, J. P. *et al.* Multivalency Amplifies the Selection and Affinity of Bradykinin-Derived Peptide for Lipid Nanovesicles. *Mol Biosyst* **9**, 2005 (2013).
205. Gori, A. *et al.* Membrane-binding peptides for extracellular vesicles on-chip analysis. *J Extracell Vesicles* **9**, (2020).
206. Loebel, C. *et al.* Metabolic labeling of secreted matrix to investigate cell–material interactions in tissue engineering and mechanobiology. *Nature Protocols 2022 17:3* **17**, 618–648 (2022).
207. Tong, M., Smeekens, J. M., Xiao, H. & Wu, R. Systematic quantification of the dynamics of newly synthesized proteins unveiling their degradation pathways in human cells. *Chem Sci* **11**, 3557 (2020).
208. Li, Y., Zhao, L. & Li, X. F. Hypoxia and the Tumor Microenvironment. *Technol Cancer Res Treat* **20**, (2021).
209. Petrova, V., Annicchiarico-Petruzzelli, M., Melino, G. & Amelio, I. The hypoxic tumour microenvironment. *Oncogenesis 2018 7:1* **7**, 1–13 (2018).
210. Salomon, C. *et al.* Exosomal Signaling during Hypoxia Mediates Microvascular Endothelial Cell Migration and Vasculogenesis. *PLoS One* **8**, e68451 (2013).